NOTA: anche questa pagina bianca fa parte del blocco di pagine della tesi

NOTA: tagliare il blocco di pagine della tesi (stampata fronte-retro) lungo le due linee qui tracciate prima di effettuare la rilegatura

UNIVERSITÀ DEGLI STUDI DI CATANIA
Dipartimento di Ingegneria Elettrica Elettronica e dei Sistemi

Francesco Pagano

SMART SYSTEMS BASED ON ELECTROACTIVE POLYMERS

Doctor of Philosophy Thesys in Ingegneria Elettronica, Automatica e del Controllo dei Sistemi Complessi

(XXV Cycle)

Coordinatore:
Chiar.mo Prof. Ing.
Luigi Fortuna

Tutor:
Chiar.mo Prof. Ing.
Salvatore Graziani

ACKNOWLEDGMENTS

Thanks goes to my family for encouraging and supporting me through my graduate and undergraduate career.

A great deal of thanks is owed to Prof. Salvatore Graziani for its input on my research.

Finally I would like to thank everyone I worked with at University of Catania for the help they provided.

CONTENTS

Abstract

The purpose of this thesis is the development and analysis of smart systems based on electroactive polymers (EAPs). Thanks to their sensing and actuation capabilities, devices based on EAPs, like ionic polymer–metal composites (IPMCs), realized by using a noble metal or ionic polymer–polymer composites (IP^2Cs), where a conducting polymer replaces the metal, pave the road to the development of new integrated devices , being the conditioning circuitry very simple, that could be of high interest in fields such as engineering, biomechanics, aerospace, and robotics. Furthermore, in the near future the entire system, included the conditioning circuitry, could be realized by using plastic based electronics, opening new possibilities for a post-silicon era.

Characteristics like the large deformations obtained under the effect of a low level applied voltage signal, the capability to transform a mechanical stimulus into a detectable electrical signal and the vibrational characteristics of a cantilever beam, have contributed to selecting the IPMC as candidates for the research carried out.

The idea that drove this thesis is to proof the possibility to use EAPs to realize a smart systems that can both perform measurements in harsh environments while being energetically self-sufficient.

This has prompted the design, the realization and the test of sensors, such as a seismic sensor and a viscometer, and of a device able to harvest energy from ambient vibrations.

This work has allowed to assert that, although the technology used is still room for improvement, this idea is feasible.

Chapter 1
INTRODUCTION

1. Ionic Polymer-Metal Composites (IPMC)

In the last decade a new breed of polymer has emerged which responds to external electrical stimulation by displaying a significant shape or size displacement. These materials known as electroactive polymers, or more commonly EAPs, are now on the verge of many exciting applications.

There are two major categories of EAPs, depending on their mode of activation mechanism, these include, electronic and ionic categories. Coulomb forces drive the electronic EAP, which include electrostrictive, electrostatic, piezoelectric and ferroelectric materials. Electronic EAP can operate in room conditions for long periods of time, they have rapid response time (in the range of milliseconds), can hold strains under DC activation. Generally, these EAP materials exhibit a greater mechanical energy density than the ionic EAP, however, the electronic EAP require high activation fields (50-150-V/μm) that may be close to the breakdown level. Ionic EAPs are materials that involve mobility or diffusion of ions. They requires low voltage and exhibits large bending displacements. Their disadvantages include a need to maintain wetness and difficulties to sustain a constant displacement under activation of a DC voltage (except for conductive polymers) and the relatively low actuation force induced.

1.1. IPMCs

This thesis is focused on IPMC, that are ionic EAP made of an ionic polymer membrane metallised on both sides with a noble metal.

The ionic polymer adopted usually consists of fixed covalent ionic groups. Typical ion exchange polymers are the following [1], [2]:

- *Perfluorinated alchenes*: polymers with short side-chains terminated by ionic groups (typically sulfonate or carboxylate SO_3^- or COO^-) for cation exchange or ammonium cations for anion exchange (Figure 1.1a). The large polymer backbones determine their mechanical strength. Short side-chains provide ionic groups that interact with water and the passage of appropriate ions.
- *Styrene/divinylbenzene-based polymers*: in these polymers the ionic groups have been substituted from phenyl rings where the nitrogen atom is fixed to an ionic group. These polymers are highly crosslinked and are rigid (Figure 1.1b).

In perfluorinated sulfonic acid polymers there are relatively few fixed ionic groups. They are located at the end of side-chains so as to position themselves in their preferred orientation to some extent.

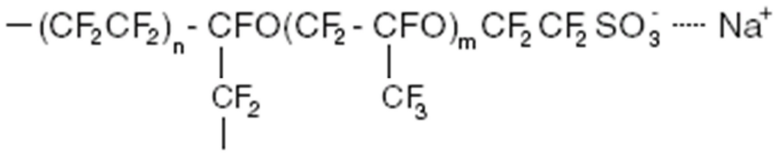

(a)

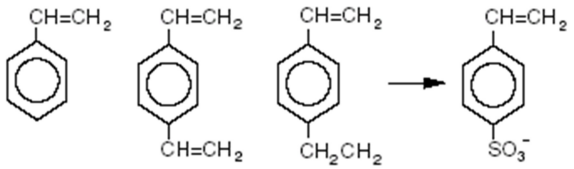

(b)

Figure 1.1: (a) Chemical structure of a Perfluorinated sulfonic acid polymer; (b) Chemical structure of Styrene/divinylbenzene-based ion exchange material.

Therefore, they can create hydrophilic nano-channels, so-called *cluster networks*.

There are several commercial ion exchange materials manufacturers; the most popular products that have been used for IPMCs fabrication are: Neosepta® from Tokuyama, Flemion® and Selemion® from Ashai Glass, and Nafion® from DuPont. Among all ionic polymer films, the most used is Nafion® 117 from DuPont, which is a perfluorosulfonate polymer (the chemical structure is reported inFigure 1.2). In particular, it is a copolymer of Tetrafluoroethylene and Sulfonyl Fluoride Vinyl Ether containing as fixed group the $-SO_3^-$ group while M^+ is the positive ion (cation) that is free to move. M^+, as furnished by the farm, is H^+ but it can be substituted, by chemical processing, with Li^+, Na^+ etc.

The most popular way of plating the polymer is an impregnation/reduction process that results in a conductive metal electrode on the surface of the polymer [3]. This process replaces the cationic groups of the polymer with a conductive metal. A reduction agent allows to form a network of metal particles on the surface of the polymer [4].

Because of the presence of the metal deposited on the surface of the polymer to facilitate electrical signal transmission to and from the polymer, they are often referred to as IPMC (Ionomeric Polymer-Metal Composite). In literature they are also called ICPF (Ionic Conducting Polymer Film), IPT (Ionic Polymer Transducer) and IMPC (Ionic Metal-Polymer Composite).

In the 1990s, interest in ionic polymer transducers increased and the material was studied for its actuation and sensing capability

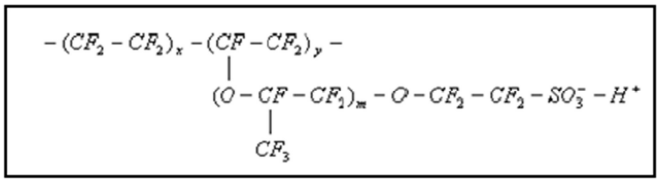

Figure 1.2: Chemical structure of Nafion®

1.2. IPMC Actuating and Sensing Mechanism

Ionic polymers have inner ionizable groups that have the properties of dissociate in a variety of solvent media and movement in the molecular net generating a strong electric field (~10^{10} V/m).

The $-SO_3^-$ group is the fixed group in the polymer matrix of Nafion® while the cation is free to move. Cations and anions move in opposite directions when a voltage is applied to a simple electrolyte and, therefore, no energy is transferred from the molecular network to the solvent, and no solvent molecule is carried. Instead, in the polymeric membrane mentioned earlier on, the solvent molecules can be parasitically carried by the free ions. Then it is clear that the deformation of an IPMC actuator is strictly linked to the charge migration inside it.

When an external voltage is applied across the thickness of the membrane, mobile cations will move toward the cathode. Moreover, if hydrated sample is considered, the cations will carry water molecules with them [5]. The cathode area will expand while the anode area will shrink; consequently the polymer will bend toward the anode. Cations with a high hydration number will produce greater deformation than cations with a low hydration number. An example is the case of the Lithium ion of which the hydrated volume is far bigger than either H^+ or Na^+ [2]. For this reason in motion-related applications, the Hydrogen ion of the Nafion® molecule can be purposefully substituted via an ion exchange process with Na^+, Li^+ etc.

The previously described phenomenon is known as water pumping. The cathode area expands while the anode area contracts. Consequently, the polymer will bend toward the anode and, of course, the larger is the number of parasitically carried water molecules, the higher the deformation effect will be (Figure 1.3). Water pumping is not the only phenomenon involved in the bending deformation when the IPMC is subjected to an electric field. Indeed, the two deposed metallic layers amplify the deformation by adding a Coulombian effect due to the interaction of the charges.

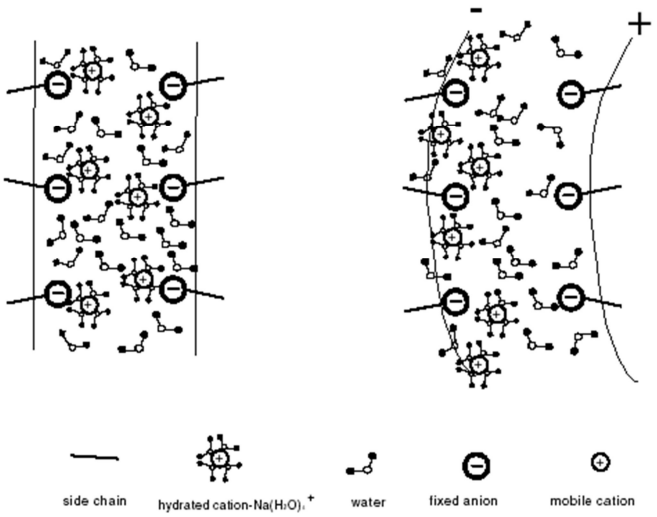

Figure 1.3: Schematic diagram of ion transport in IPMCs

After deposition, the metallic ions scatter everywhere through the surface regions of the polymer because of the latter porous structure, and then they are reduced to their metallic atoms: the result is the formation of dendritic electrodes [5]. Moreover an external voltage will produce the accumulation of opposite charges on the two electrodes so the charges will interact with fixed anions in the polymeric bulk; these two effects are schematically shown in Figure 1.4. It is interesting to note that the interaction will be attractive for one electrode and repulsive for the other. This effect is responsible for a further bending deformation due to the differential contraction–expansion of the strip's external fibres. Dendritic electrodes act as if the charges were concentrated at their ends.

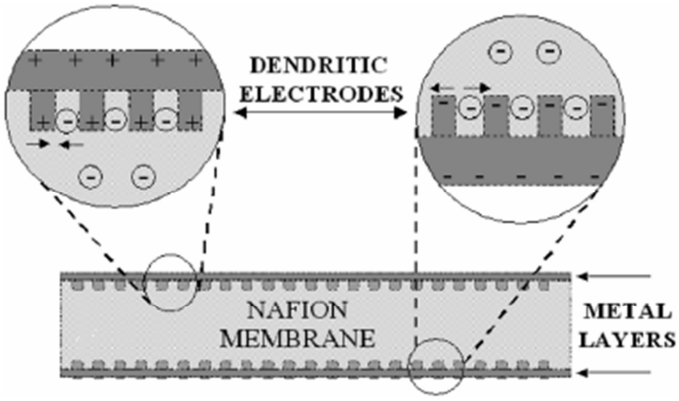

Figure 1.4: Interaction of charges within the IPMC membrane

The interaction with fixed and mobile ions of the network occurs only close to the upper and lower surfaces of the strip.

When a constant voltage is applied, the gradient of water concentration causes a back diffusion of the water molecules that, in turn, is responsible for the relaxation of the membrane and the production of a residual deformation . As a consequence, IPMCs are not able to maintain large constant deformations [6].

Water back diffusion is not the only cause of the membrane performance degradation over time. One must also consider that water tends to escape from the membrane both because of evaporation and of water electrolysis. Continuous membrane hydration has to be provided if constant performance is required.

The sensing capability has been demonstrated by measuring the inverse performance, i.e. the voltage produced by the transducer when a deformation is forced [4]. The relationship between induced current in the polymer has been shown to be proportional to the mechanical deformation [2].

A parameter that quantifies the sensing performance of the polymer is the electromechanical sensitivity of the material. In 2003, Farinholt *et al* [5] measured the sensitivity of Nafion® when a bending, shear, or tensile force was applied. The material was found to be most sensitive to an imposed bending force.

The bending sensitivity of the material is dependent upon several factors. The frequency of the applied force, the length of the transducer, and the ionic form of the material has an effect on the electrical response of the polymer [6]. A comparison of the polymer with different cation clusters in the material indicates that the bending sensitivity increases with the ionic size of the material.

1.3. IPMC Modeling

Researcher involved in the study of IPMC adopted different modelling approaches so that a number of models have been proposed in the literature. Currently there are three modelling approach for IPMCs: black box models, white box models, and grey box model [7], [8], [9].
The first (black box modelling) offers the least amount of insight into the fundamental mechanisms and is referred to as the black box model. This modeling technique provides a purely empirical model of IPMCs obtained through a series of curve fits based on experimental data [10], [11]. The first black box model of IPMCs was developed in 1994 by Kanno et al. [10]. Their model, shown in Eqn.(1.1), offers nine fit parameters that can be used to fit experimental results.

$$Y = Ae^{-\alpha t} + Be^{-\beta t} + De^{-\gamma t} + Ee^{\delta t} + F \tag{1.1}$$

They found that the parameters could not describe each excitation level, thus making the model dependent on both sample geometry and excitation voltage.

Xiao and Bhattacharya [11] also proposed a black box model of the ionic polymer transducer, focusing on the curvature of the IPT sample as it evolves with voltage and time. Their model is shown in Eqn (1.2):

$$\frac{d\kappa}{dt} = \frac{1}{\tau}\left(\kappa_v V - \kappa\right) \tag{1.2}$$

where κ is the curvature of the sample, κ_v is the saturation curvature per volt, τ is the time constant, V is the applied voltage and t is the time variable. Interestingly, their development begins with more of an electrostatics development, however when placed in the reduced

form used to model the macroscopic response of the IPT, they revert to a phenomenological model of the eigen-curvature.

This kind of models was first developed when there was very little knowledge of ionic polymer dynamics but a need for a model able to estimate the IPMC behavior for various applications was largely reported.

The second type of models – called white box models, or physical models – rely on the underlying physical mechanisms of the IPMC to develop a system of equations that fully describe the material response [12], [13], [8]. These type of models attempts to describe the underlying microscopic physics and resulting transducer response. These models are not usually well suited for engineering applications because of the complexity of the resulting equations. Nemat-Nasser and Li [12] proposed a micromechanics model based on coupled three dimensional field equations. The constitutive parameters in the model are estimated based on the microstructure of the transducer using micromechanics. Nemat-Nasser and Li [12] proposed that the cations in the transducer migrate under an applied field and the anions that are attached to the backbone of the polymer move in an attempt to rebalance the local charge, this electrostatic motion creates the motion of the polymer and water migration and hydrostatics are secondary phenomena. This explanation of actuation is much different than the treatment of Tadokoro *et al.* [8], where the water migration was the primary cause of motion. Nemat-Nasser and Li [12] explain sensing in ionic polymers by the stress created by motion displaces the charge centre of the ionic cluster and the resulting dipole creates a voltage across the electrodes of the transducer. The equations needed to describe an ionic polymer transducer in this model are much more complicated than is desirable for engineering applications of ionic polymer transducers. Since then, Nemat-Nasser has focused on the micro-mechanics associated with the phenomenon of actuation in ionic polymers [13]. Another example of white-box model is the model proposed in Tadokoro *et al.* [8]. This model is based on the relationship between three transducer properties, electrical, stress generation, and mechanical. Tadokoro *et al.* [11] proposed that a voltage applied to the transducer causes mobile cations to move from the anode (positive) to the cathode (negative) side of the transduc-

er, pulling water with along too. This water distribution causes the swelling of one side and the shrinking of the other, creating a curvature of the sample. Removal of the voltage redistributes the cations and pulls water again causing a motion in the opposite direction as the initial motion. This model results in a system of coupled partial differential equations that can be simplified and solved. The equations are composed of relationships between physical and chemical parameters not well understood or directly measurable. They did however show good correlation between measured data and predicted motion.

These two types of models both have drawbacks from an engineering design standpoint. The first type lacks the scalability and physical relevance of terms, the second lacks simplicity and macroscopic relevance of the terms and equations involved. The ideal design model would consist of easily obtainable material properties and easily measurable transducer dimensions.

The third approach is considered the more enlightening grey box modeling. Still based somewhat on empirical data, grey box models combine fundamental physical laws with empirically derived parameters to describe IPMC electromechanical conversion. The empirically determined parameters often correspond to processes or mechanisms that are not as well understood or too complex to be incorporated into the grey box models [7], [9], [14], [15], [16].

The first of these grey box models was proposed in 1996 by Kanno *et al.* [14] in which he divides the model into two subsections: the electrical and the stress generation stages. Using an equivalent circuit model of the IPMC, Kanno *et al.* develop a relationship that describes the electrical current that is developed from an applied voltage. This portion constitutes the electrical stage whose output, the current, represent the input to the stress generation or mechanical stage of the model.

Work by De Gennes *et al.* [7] relies on a model formulation that has the potential to describe both sensing and actuation responses, however their consideration of only steady-state results does not account for the transient field developed in sensing. Their model is based upon linear irreversible thermodynamics and relates the flux terms of electrical and water current to the driving forces of electric field and water pressure.

While offering a very concise representation of the system, deGennes *et al*. [7] unfortunately do not compare their predictions with the measured performance of IPMCs.

Another grey box model has been proposed by Paquette *et al*. [17]. The authors continue along the development of de Gennes *et al*. [7], presenting an equivalent electrical circuit of the IPMC that characterizes the upper and lower electrode surfaces as well as the bulk polymer membrane. This model assumes that the membrane is purely capacitive and that the upper and lower electrodes exhibit RC characteristics. The model enables Paquette *et al*. [17] to model the current to voltage relationship in an equivalent circuit form. The concept is then integrated into the irreversible thermodynamics model of de Gennes *et al*. to provide predictive capabilities for the blocked force response of the IPMC.

Newbury [9] and Newbury and Leo [15] propose a linear two port model that can be used for modelling both actuation and sensing properties of a cantilever actuator or sensor. The energy conversion between the electrical and mechanical domains can be represented using an ideal linear transformer where the electric quantities are on one side of the transformer, and the mechanical quantities are on the other side, as shown in Figure 1.5

The model proposed in Newbury [9] and Newbury and Leo [15] provides a linearly coupled set of equations that allow scaling of transducers and their performance prediction without having to redetermine parameters in the model.

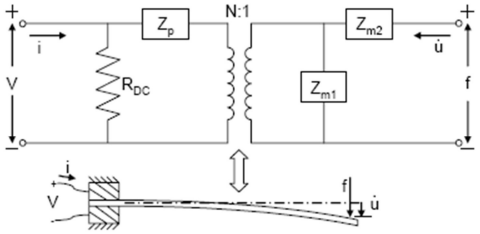

Figure 1.5: The model of Newbury and Leo

The terms in the equations contain measurable macroscopic physical and electrical properties of the transducer as well as its geometry. Material parameters include the Young modulus, density, and electrical permittivity. This allows the scaling of transducers without having to redetermine coefficients in the equations. This model allows the prediction of various input-output relationships and was validated for different transducer sizes for a frequency range of up to 20 Hz. The model does not try to explain or incorporate the fundamental phenomena within the transducer but rather provides an engineering model useful in the design and application of ionic polymer transducers. One of the limitations with this model is the relatively low frequency range of validation; higher frequency exploration has not been performed. Using a similar approach, Bonomo et al. [16] developed a model able to predict also the nonlinearities in the input absorbed current, introducing two diodes, as shown in Figure 1.6. These diodes are described by adapting the Shockley ideal diode equation.

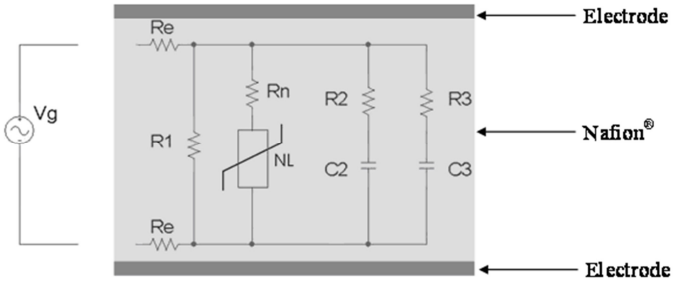

Figure 1.6: The equivalent electrical circuit for an ionic polymer metal composite based actuator proposed by Bonomo et al

The mechanical response of the actuator is induced by the current passing through the branches R2-C2, R3-C3, reflecting the capacitive nature of IPMC.

Although numerous possible applications of ionic IPMCs in underwater environment, few models have been proposed in the literature for such environments.

In the next section a literature review about the possible applications is reported.

1.4. IPMC Applications

The most attractive feature of EAP materials is their ability to emulate biological muscles with high fracture tolerance, large actuation strain and inherent vibration damping. EAP actuation similarity to biological muscles gained them the name "Artificial Muscles" and potentially can be used to develop biologically inspired robots. The limited force actuation of current EAP is constraining the practical applications that can be considered. Since EAP can be used as actuators that are light, compact and driven by low power, it is possible to take advantage of their resilience and fracture toughness to develop space applications, and in general applications in which high force are not required, as those proposed in this thesis.
In the following some potential applications realized by using IPMCs materials in the biomedical and industrial field are reported.

Microgrippers are essential tools in industrial processes. An integrated microgripper system, which can be easily implemented with any platforms operated with objects having a wide range of sizes and shapes, will have a great impact on micro-optics manipulation, micro-electro-mechanical systems (MEMS), fiber-optics assembly, biomedical manipulation, and semiconductor manufacturing. K. S. Yun in his dissertation proposed, a micro gripper realized with IPCM and based on a specific control scheme. It will have significant applications including picking-and-placing micro-sized objects or as medical instruments. The precise manipulation of this three-finger gripper was successfully demonstrated with experimental closed-loop responses. A picture of the realized gripper is shown in Figure 1.7.

A more recent version of micro gripper realized with IPMC has been proposed. More specifically a remote center compliance (RCC) device that controls micro assembly operations [2], [12], [13], [18], [19], [20], consisting of a micro gripper with manipulation arm, has been realized by using 4 IPMCs strips [21]. The micro gripper consists of three IPMC fingers linking to the wrist and a single IPMC strip used as flexible low force robotic arm, as shown in Figure 1.8. The system allows lifting micro object with small alignment in either position or orientation inde-

pendently. Insertion depth decrease with alignment angle and increase with applied voltage, as shown inFigure 1.9.

Figure 1.7: CAD model of RCC based micro gripper using IPMC

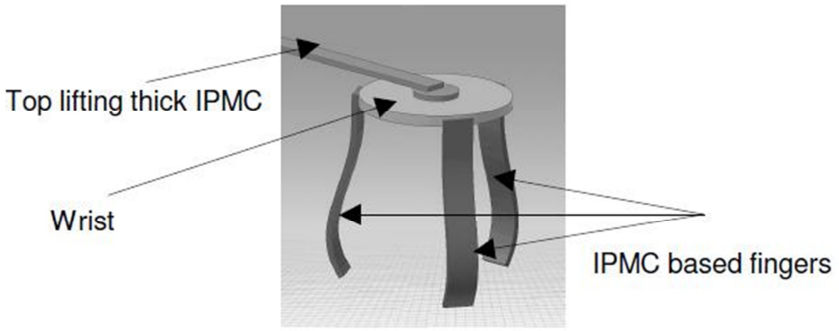

Figure 1.8: CAD model of RCC based micro gripper using IPMC

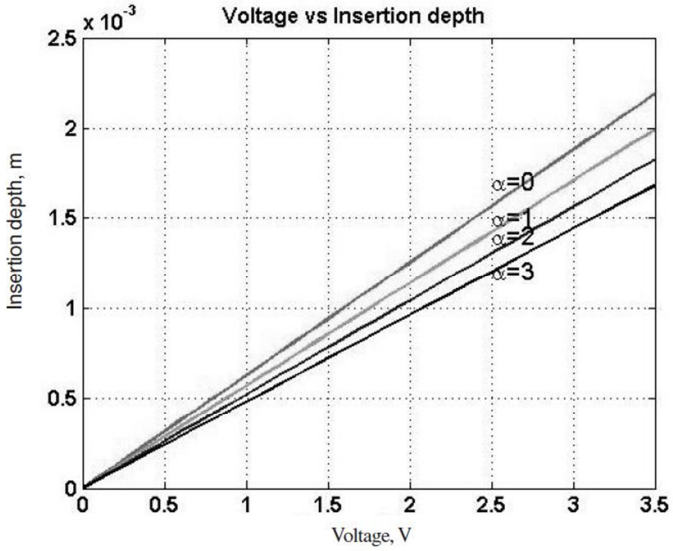

Figure 1.9: Performance of insertion depth of micro robotic arm and voltage

A lot of underwater robot that involve IPMC as actuator have been proposed in literature, being these materials suitable to work in aqueous environment. One of the first robot proposed is a robot that mimics rajiform swimming by undulating motions of pectoral fins. The realized prototype, showed in Figure 1.10 has two pectoral fins, composed of two IPMC sheets connected by a plastic foil. The tests confirmed that the fins are able to generate thrust and move the robot forward.

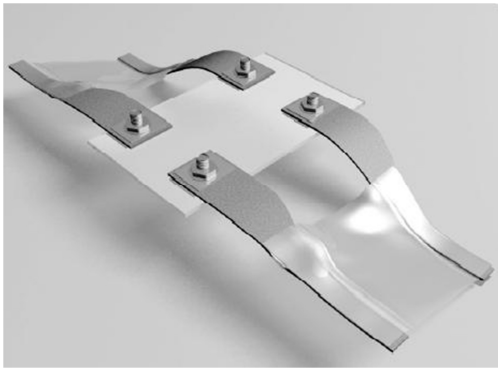

Figure 1.10: Computer generated image of the robot with two pectoral fins.

A more recent version of this model has been proposed by M. Yamamura et al. and it is shown in Figure 1.11. From the figure it is possible to notice that 8 IPMC strips are used for each fin. A simple traveling wave input generates propulsion of the fins.

In Figure 1.12 another robotic fish design is presented [2]. This robotic fish, equipped with a tail fin made from a single piece of IPMC material, has demonstrated that such a structure is feasible for mimicking biological fish locomotion.

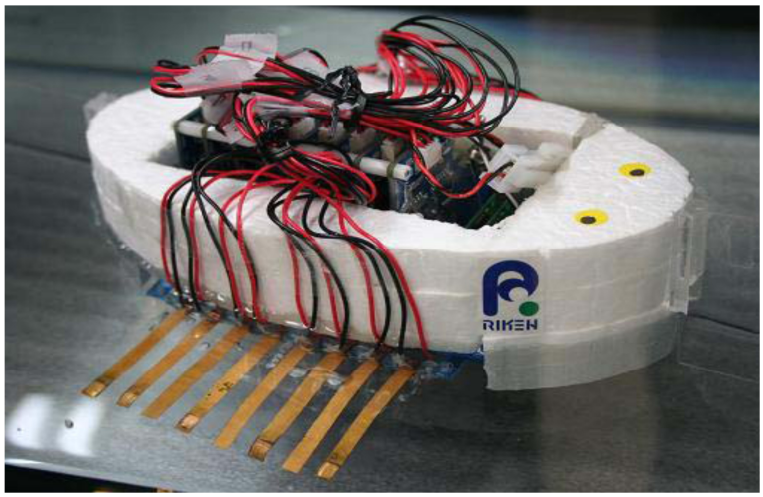

Figure 1.11: Aquatic robot with 8 IPMC strips for each fin

Furthermore, the noiseless propulsion is attractive in nature. A maximum speed of approximately 2 m/min was achieved under an applied voltage of 2 V.

Micropumps are devices that can be easily realized by using IPMC sheets. Bellows pumps can be made by attaching two planar sections of slightly different sizes of IPMC sections and properly placing electrodes on the resulting cavity. This permits modulation of the volume trapped between the IPMCs. The applied voltage amplitude and frequency can be adjusted to control the flow and volume of fluid being pumped. IPMC diaphragmpumps can also be made in various ways. Single or multiple IPMCs can function as the diaphragms that create volume displacement.

Figure 1.12: Robotic fish equipped with a single IPMC tail fin

In Figure 1.13 a miniaturized double-diaphragm pump constructed of IPMC is shown. Such a pump produces no noise and has a controllable flow rate in the range of a few microliters per minute. These pump systems can also be useful for biomedical applications. For example, each includes a pumping chamber having an anterior end attached to an implantable influent conduit in eye. In the case of an ocular pressure control device, the influent conduit is inserted into the anterior chamber of the eye. A flexing ionic polymer conductor composite IPMC artificial muscle functions as the primary actuator. The posterior end of the pumping chamber is connected to an effluent or drainage conduit, which may drain bodily fluids or dispense drugs to an area of the body. Figure 1.14 depict various configurations of such mini diaphragm pumps with rectangular and circular chambers.

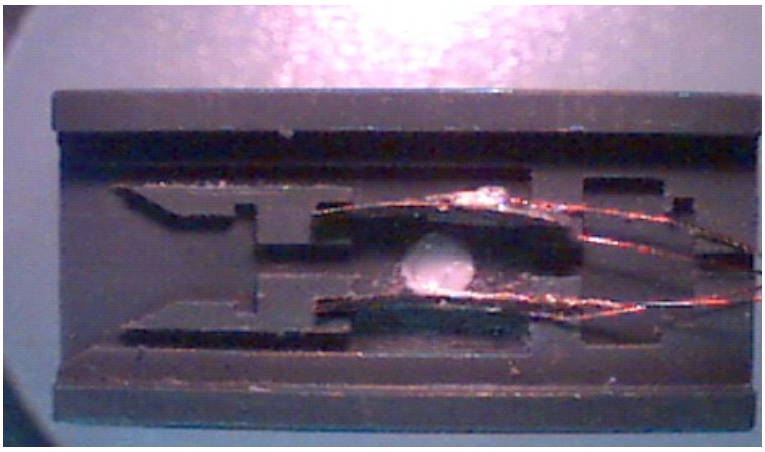

Figure 1.13: A photograph of the fabricated double-diaphragmpump. The size of the IPMC is 1 mm width × 5 mm length × 0.2 mm thickness [2].

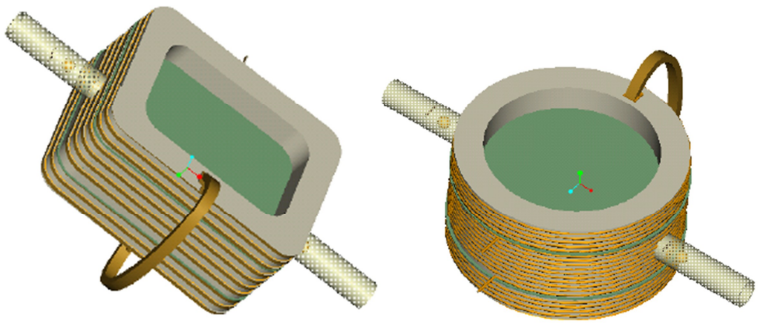

Figure 1.14: Perspective view of two (rectangular and circular chamber) double-diaphragm mini-pumps equipped with IPMC muscles and an inductive receiving coil

A low cost and reliable IPMC actuator applicable to the development of disposable active cardiac catheter was designed and fabricated in [22] (Figure 1.15). An empirical model of the IPMC actuator for aqueous manipulation was constructed. The model consisted of a fourth-order transfer function, a nonlinear gain and a time-delay term. Its parameters were varied with driving potential, operating time and frequency. With the nonlinear compensation method proposed, the model was linearlized and the actuator performed well under the conventional PID closed-loop controller in bending angle control experiments.

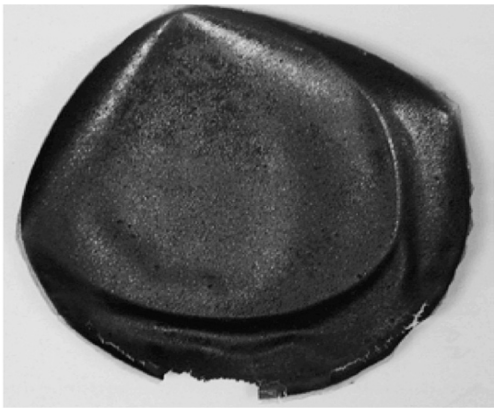

Figure 1.15: IPMC fpr the realization of an active catheter systems

2. Ionic Polymer - Polymer Composites (IP²C)

As mentioned above IPMCs are constituted by an ion exchange perfluorinated membrane, coated on both sides with a metallic electrode, generally a noble metal such as platinum or gold [1]. These metals are characterized by high cost and require complex deposition techniques in order to obtain the electrodes. For the reasons mentioned above, all-organic transducers, with electrodes realized by using organic conductors [23], [24], [25], [26], [27], named ionic polymer–polymer composites (IP²Cs), have been introduced.

This new class of transducers exploits polymers that are becoming available and that are characterized by high conductivity values. They have already attracted researcher's interest in various application domains from electronics to robotics or biochemistry organic conductors.

All-organic actuators and sensors have been realized based on a fluorocarbon membrane (i.e. Nafion 117), covered in both sides by a conductive material.

The basic procedure in fabricating IP²Cs comprises five main steps:

1. A sandblasting step is required to ensure mechanical adhesion of the organic conductor (since rough samples guarantee better adhesion properties)
2. Ultrasonic cleaning, in order to remove material residues

3. Chemical cleaning (by boiling in HCl (2.5 M) and, then, water).
4. The organic conductor is deposited using techniques such as *spin-coating, dip-coating, spin-casting* and *printing techniques*
5. After solvent evaporation, the obtained samples are immersed in deionized water.

The deposition techniques of organic materials from solutions are relevant due to their low manufacturing cost. The conducting materials usually used to realize the IP²Cs are listed in Table 1.1.

Table 1.1: Conducting materials

Organic Conductor	Trade Name	Producer
PEDOT:PSS	Baytron® PH 500	H.C. Starck
PEDOT:PSS	Baytron® P HC V4	H.C. Starck
PEDOT:PSS	Orgacon™ EL-P 3040	AGFA
PEDOT:PSS	Orgacon™ EL-P 5010	AGFA
PANI	Polyaniline (Emeraldine Base) Mw - 50000	Sigma Aldrich

Figure 1.16 shows a sample of IP²C prepared by using the drop-casting technique.

Figure 1.16: Samples prepared by drop-casting technique.

In Figure 1.17 four SEM images of two IP²C sections are reported. More specifically, figures (c) and (d) show two samples with Orgacon® EL-P 3040 electrodes, whose thickness is about 6–7 μm, while the thickness of the Nafion® 117 membrane is 178 μm. It is possible to observe that the PEDOT:PSS surface is highly inhomogeneous. Moreover, the electrode thicknesses of two devices with the same organic conductor can be different because of the conductor deposition process, as shown in Figure 1.17.

In the following of the thesis both IPMC and therefore IP²C transducing performance are exploited to realize post-silicon devices.

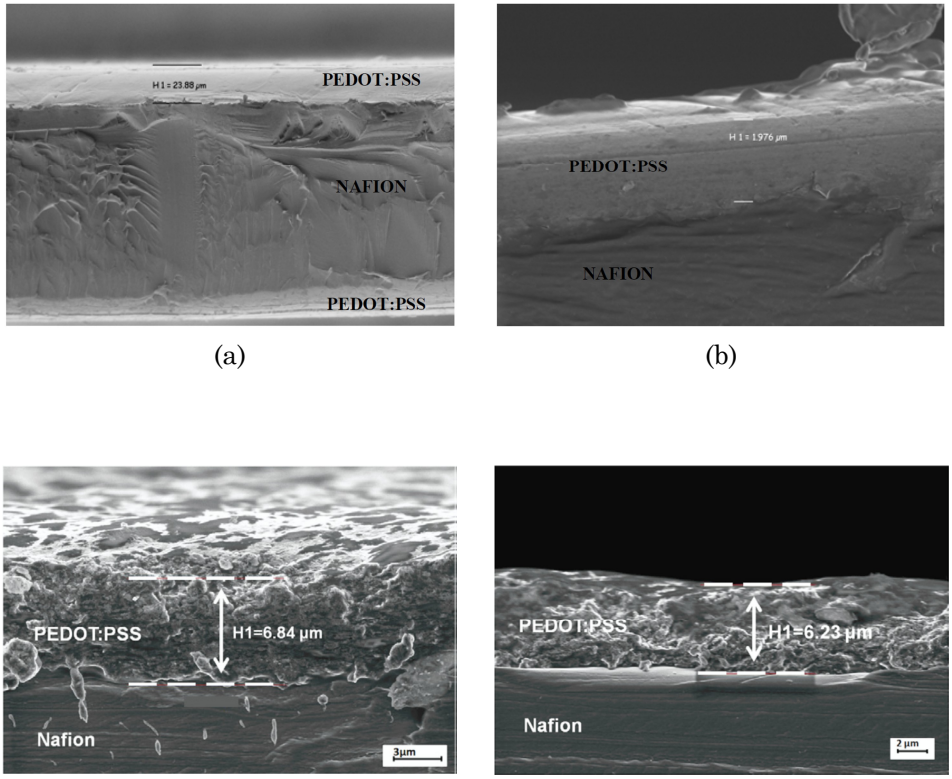

Figure 1.17: SEM images of a section of dip coated PEDOT:PSS film.

3. Experimental Set-up

Analysis of the behaviour of the proposed systems usually involves three main stages:

1. design and construction of an experimental setup able to electrify the membranes under study and reproduce the environmental conditions
2. measurement campaign

3. processing of the collected resultant digital signals to extract the particular information required

The research described below, depends on the use of some external devices both to digitize and analyse the signals. Among the most important can be mentioned:

- Distance laser sensor 12U6460/S35A Baumer Electric.
- Shaker (Tira TV 50009)
- copper electrodes realized on a printed board. (Figure 1.18)

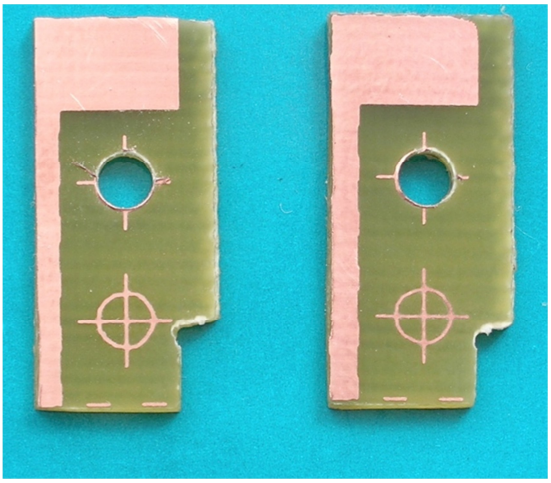

Figure 1.18: copper electrodes realized on a printed board

There is now a very wide range of ADC cards available for operation in PCs for the acquisition of data The systems used is based on the National Instruments data acquisition card model NI-PCI 6052E.

The interactions with the users were guaranteed thanks to the use of a dedicated interface developed in the Labview® environment.

In practice, most of the experiments require purpose-designed software. These will include (see later) spectral analisys, system's transfer function calculation, estimation of the predicted signals for the systems under investigation.

The analysis of the signals obtained took advantage by using a PC-based systems with the software MathWorks Matlab®.

3.1. Conditioning circuitry

Considering IPMC and IP²C based systems, in an electrically view, the critical point for these systems is not the high frequency, which in fact does not exceed 100 Hz, but the low level of the output signal. In fact, due to the small signal found, a specially designed signal conditioning circuitry was realized.

Main characteristics of these circuits are an high gain and a low noise floor.

In Figure 1.19 the conditioning circuits for the IPMC actuator and sensor are shown.

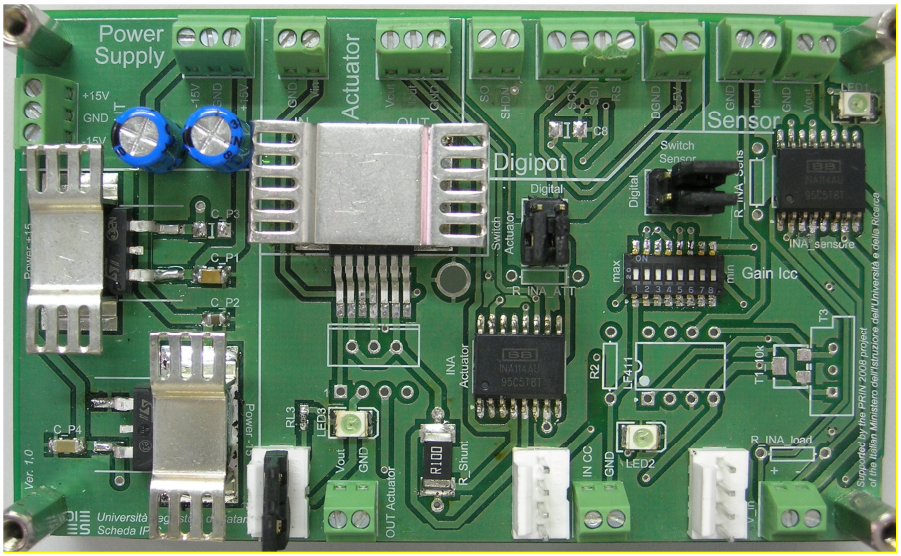

Figure 1.19: Real view of the conditioning circuits

3.1.1. Conditioning circuit of the IPMC sensor

Figure 1.20 reports the scheme of the circuit adopted for the estimation of the short circuit current of the IPMC sensor.

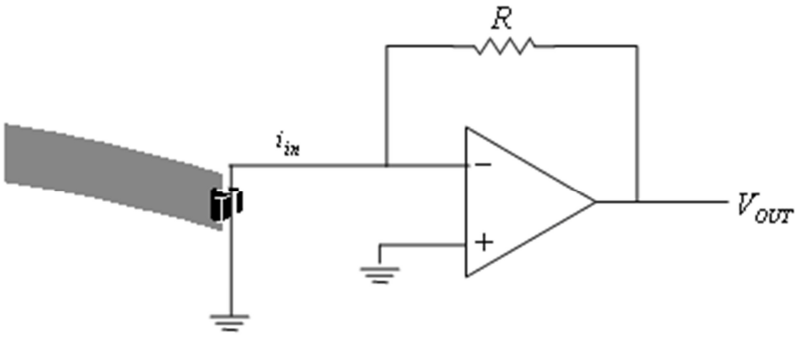

Figure 1.20: The scheme of the conditioning circuit of the IPMC sensor

The sensor's conditioning circuit is a short circuit current amplifier. The IPMC sensor generates currents of the order of magnitude of micro-amperes. Consequently, in order to ensure the output voltages in the order of a few volts, the gain of the amplifier must be sufficiently high, approximately 10^6.

This gain is linked to the value of the feedback resistor R as shown in Figure 1.20.

The relation between the output voltage and the input current is given by Ohm's law.

$$V_{OUT} = -RI_{in} \tag{1.3}$$

The presence of a gain so high imposes the necessity to adjust the amplifier offset. In fact, the presence of a DC component in the input signal could saturate the obtained output signal.

The operational amplifier used allows the offset adjustment through insertion of a trimmer appropriately positioned.

Bending a IPMC used as a sensor, by both sides with respect to the longitudinal axis both negative and positive, currents are produced. It is therefore necessary to use a dual power supply. A dual voltage ±15 V ensures that the output signal can be positive or negative following the direction which the IPMC is deflected.

3.1.2. Conditioning circuit of the IPMC actuator

Figure 1.21 reports the conditioning circuit adopted for the driving of the IPMC actuator along with the INA111 (instrumentation amplifier) for the estimation of the absorbed current of the IPMC actuator.

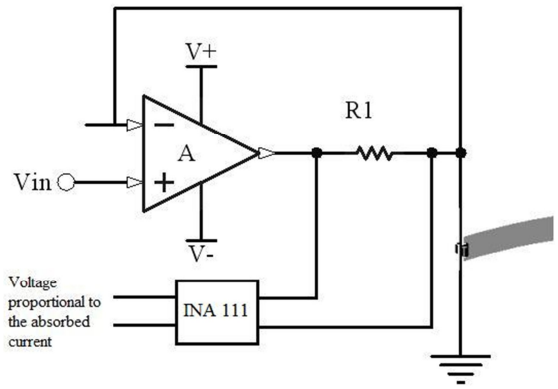

Figure 1.21: The scheme of the conditioning circuit of the IPMC actuator

The conditioning circuit for an IPMC used as actuator must to be able to provide the suitable level of current, required for the proper functioning of the device.

During its normal operation, the IPMC actuator requires a voltage in the range [0, 2 V - 6 V]. The levels of current drained during the operation of the actuator are extremely variable and depend, as well as by the amplitude of the control signal, also by the dynamics of the external signal imposed.

In order to ensure the functioning of the IPMC actuator, even in extreme conditions a power operational amplifier OPA548 capable of deliver a maximum continuous current of 3.0 A and 5.0 A of peak current was used.

A INA111 has been inserted into the circuit to measure the absorbed current , it is able to detect the voltage drop, caused by the current absorbed by the actuator, on a shunt resistor R1 in series with the IPMC output.

Thanks to this voltage it is possible to trace the current that flows in the operational amplifier output

$$I_{OUT} = \frac{V_{INA}}{R_{shunt}\, G_{INA}} \tag{1.4}$$

where I_{OUT} represent the output current value, R_{shunt} represent the value of the resistance in series with the amplifier output and G_{INA} represent the gain of the INA111

Chapter 2
A SMALL SCALE VISCOMETER BASED ON IPMC

1. Introduction

In the last years the use of cantilevers in rheological measurements of fluids has received a big attention [28], [29], [30]. Rheological application of small-size cantilevers proposed in literature was generally restricted to the measurement of liquid viscosity [31], while a priori and independent measurement or knowledge of the liquid density was required, which restricts the utility of this technique.
Sader et al. developed a theoretical framework [32], [33] for the description of cantilever vibrations in viscous fluids. That theory can be exploited for the simultaneous measurement of both density and viscosity of fluids [31]. Here a system is proposed that exploits the electromechanical characteristics of a vibrating system at its resonance frequency to determine the density and the viscosity of the fluid in which it is immersed. In particular, use the frequency response of a cantilever immersed in a fluid, allows to estimate the rheological properties of the fluid. More specifically, a device that uses the frequency response of two IPMC strips fixed together in cantilever configuration in order to estimate both the density and viscosity of liquids is proposed.

All the properties mentioned above make IPMCs suitable for the viscometer envisaged here.

Thanks to the use of an IPMC strip as an actuator and an IPMC strip as a sensor, the viscometer is very simple in structure and opera-

tion modality and will be easy to be micro manufactured; moreover, it requires a low-voltage supply and it is lightweight.

The considerations reported above show the interesting properties of the IPMC based small scale viscometer.

More specifically, the possibility to use IPMCs for viscosity and density measurements of sucrose solutions is demonstrated. Sugar solutions are valuable test systems for such devices, since many biological liquids contain a remarkable amount of sugar [34].

In this work were realized two different versions of the viscometer.

The first version of the measuring system involved the use of an IPMC actuator, set in vibration under the effect of an external electrical force, and a commercial laser sensor [35], used to measure the corresponding deflection of the vibrating system. It was, evidently, an intermediate system, intended to verify the operating principle.

The second version of the measuring system is based on the use of two IPMC membranes, respectively used as actuator and sensor. The second IPMC strip was added in order to measure the deflection [36]. Such a system will allow to exclude the laser and obtain a device, based only on polymeric materials, capable of measuring the density and viscosity of fluids.

2. The first version

The proposed device uses the electromechanical characteristics of a vibrating system at the resonance frequency, to determine the density and the viscosity of the fluid in which it is immersed [31].

The system, in its first version, involves the use of an actuator IPMC set in vibration. The deflection produced is measured by using a laser sensor [35].

The vibration is produced by applying a sinusoidal voltage signal, that sweep across the interested frequency bandwidth, to the electrodes of the IPMC actuator which, subjected to electric stress, deflects in response to the imposed signal [37], [38].

To measure the amplitude and frequency of the deflection produced by the actuator the distance laser sensor 12U6460/S35A Baumer Electric was used.

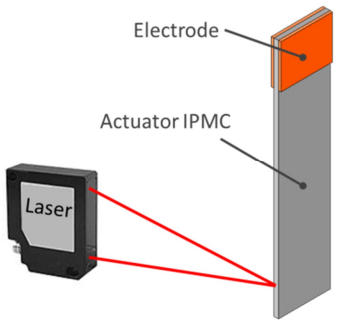

Figure 2.1: The sensing element of the device in his first version

2.1. The Model

In this section the IPMC model used to realize the viscometer is introduced. In literature a number of models of IPMC actuators has been reported [38], [39]. These models describe the behaviour of the IPMC in the absence of any fluid (i.e. in vacuum), while the modelling of an active beam immersed in a viscous fluid in not so much investigated.
An analytical model for IPMC actuators immersed in a viscous fluid [37] was used to design the viscometer. The modelling approach is based on the hydrodynamic function concept for the case of an active IPMC beam with rectangular cross-section.
The motion equation of the IPMC actuator in a viscous fluid is obtained by adding to the equation ruling motion in vacuum, the force [40]

$$g = g_V + F_h \tag{2.1}$$

where the term g_V represents the fluid damping force and the term F_h represents the inertial force, due to a skin of fluid dragged by the cantilever in its motion, that corresponds to an additional mass.

The term g_V can be expressed by

$$g_V = -C_V \frac{\partial w}{\partial t} \tag{2.2}$$

where C_V is the fluid damping coefficient, w is the beam deflection and t is the time. The term F_h can be expressed by

$$F_h = -m_a \frac{\partial^2 w}{\partial t^2} \tag{2.3}$$

where m_a is referred to as the added mass that is proportional to the displaced mass of the fluid, m_d.

$$m_a = C_m m_d = C_m V \rho_f \tag{2.4}$$

where C_m is the added mass coefficient, V is the volume of the immersed body, and ρ_f is the density of the fluid.
The system's equation of motion can be solved by knowing the value of the two constants C_m and C_V. In particular, the value of these constants can be analytically calculated considering the case of a bar with a cylindrical section and infinite length, and taking into account the Navier-Stokes equations [41], [42].
For small values of the amplitude of the oscillations, and in conditions of oscillatory motion stationary, ($w=w_0 sin(\omega t)$), the equation (2.1) can be rewritten as [40]

$$g = -C_m m_d \frac{d^2 w}{dt^2} - C_v \frac{dw}{dt} = m_d \omega^2 w_0 [Re(\Gamma) sin\omega t + Im(\Gamma) cos\omega t] \tag{2.5}$$

C_m and C_V can be computed by using the real and imaginary parts of the complex function Γ:

$$\begin{aligned} C_m &= \mathrm{Re}(\Gamma) \\ C_V &= -m_d \omega \,\mathrm{Im}(\Gamma) \\ m_d &= \rho_f (\pi/4) b^2 \end{aligned} \tag{2.6}$$

where $\Gamma(\omega)$ is the hydrodynamic function and b is the width of the IPMC cross-section.

The exact expression of the hydrodynamic function is known in the literature in the case of a beam with circular cross section and takes the following form [32]

$$\Gamma_{circ}(\omega) = 1 + \frac{4iK_1\left(-i\sqrt{iRe}\right)}{\sqrt{iRe}K_0\left(-i\sqrt{iRe}\right)} \tag{2.7}$$

where K_0 and K_1 are the modified Bessel functions of the third kind, and Re is the Reynolds number, which is

$$Re = \frac{\pi\rho_f b^2 f}{2\eta} \tag{2.8}$$

The parameter b represents the dominant dimension for the description of the motion in the fluid (the diameter for a beam with circular cross-section, the width for a beam with rectangular section).

In the case of membrane with rectangular cross section, the hydrodynamic function can be obtained starting from the expression (2.7) and using a correcting term $\Omega(\omega)$

$$\Gamma_{rect}(\omega) = \Omega(\omega)\Gamma_{circ}(\omega) \tag{2.9}$$

the expression of the term $\Omega(\omega)$ can be found in the literature [32].

The function $\Gamma(\omega)$ thus obtained is valid for values of the Reynolds number in the range $0.1 \leq Re \leq 1000$. However, for the operating conditions envisaged for the proposed device, this parameter varies in an interval much more limited [37] and it is possible to use simplified expression of the hydrodynamic function [43]. The real and imaginary parts of the proposed hydrodynamic function are, respectively,

$$\begin{aligned} \mathrm{Re}(\Gamma) &= c_1 + c_2\frac{\delta}{b} \\ \mathrm{Im}(\Gamma) &= c_3\frac{\delta}{b} + c_4\left(\frac{\delta}{b}\right)^2 \end{aligned} \tag{2.10}$$

where c_1, c_2, c_3 and c_4 are suitable parameter and δ is the length giving the thickness of the thin viscous layer surrounding the cantilever in which the velocity has dropped by a factor of $1/e$ [43] [44]:

$$\delta = \sqrt{\frac{2\eta}{\rho_f \omega}} \tag{2.11}$$

where η is the viscosity. The approximated expression (2.10) is obtained by fitting the corresponding complete form for a fixed IPMC actuator shape, in the frequency range considered. Substituting (2.10) in (2.6) the following expressions for coefficients C_m and C_v are obtained

$$\begin{aligned} C_m &= c_1 + c_2 \frac{\delta}{b} \\ C_V &= -m_d \omega \left(c_3 \frac{\delta}{b} + c_4 \left(\frac{\delta}{b} \right)^2 \right). \end{aligned} \tag{2.12}$$

The hydrodynamic function can be used to rewrite the motion equation of the IPMC actuator by taking into account its interaction with the fluid

$$\begin{aligned} &YI \frac{\partial^4 w(x,t)}{\partial x^4} + C_v \frac{\partial w(x,t)}{\partial t} + \\ &+ \left(\rho_c A + C_m \rho_f \frac{\pi}{4} b^2 \right) \frac{\partial^2 w(x,t)}{\partial t^2} = f(x,t) \end{aligned} \tag{2.13}$$

The mode summation method [45] can be used for the solution of (2.13). More specifically the motion of the IPMC actuator can be estimated as

$$\begin{aligned} &w^f(x,t) = \\ &\frac{1}{\rho_c A + m_d} \sum_i \frac{H_i^f(\omega)}{\left(\omega_i^f\right)^2} \varphi_i'(L) \varphi_i(x) M_0 e^{j\omega t} = \\ &= \frac{1}{\rho_c A + m_d} \sum_i \frac{H_i^f(\omega)}{\left(\omega_i^f\right)^2} \varphi_i'(L) \varphi_i(x) \frac{d_c(\omega)\, h\, w\, Y}{2} V_0 e^{j\omega t} \end{aligned} \tag{2.14}$$

Where:

$$H_i(\omega) = \frac{1}{1-\left(\omega/\omega_i^f\right)^2 + j2\xi_i^f\,\omega/\omega_i^f}$$

$$\omega_i^f = \omega_i\left(1+\frac{\pi\rho_f b}{\pi\rho_c h}C_m\left(\omega_i^f\right)\right)^{-1/2} \qquad (2.15)$$

$$\xi_i^f = \frac{C_v\left(\omega_i^f\right)}{2\rho_c A\omega_i^f}.$$

and M_0 is the module of the bending moment, produced by an external voltage stress with V_0 as module, through the coupling term $d_a(\omega)$ [39].

In the neighbourhood of each resonant peak, the frequency response of a cantilever beam, when the quality factor Q greatly exceeds unity, can be approximated as that of a simple harmonic oscillator [31]. The amplitude frequency response $w_i^f(\omega)$ is given by

$$w_i^f(\omega) = \frac{W_0\omega_r^2}{\sqrt{\left(\omega-\omega_r^2\right)+\omega^2\omega_r^2/Q^2}} \qquad (2.16)$$

where W_0 denotes the amplitude at the frequency $\omega = 0$, Q is the quality factor defined as:

$$Q = \frac{4\mu/\pi\rho b^2 + \Gamma_r(\omega_r)}{\Gamma_i(\omega_r)} \qquad (2.17)$$

and ω and ω_r are the radial frequencies and resonant frequency, respectively.

For the cantilever calibration and measurement of rheological parameters, equations (2.15) and (2.17) have been used.

Quantities in (2.16) and (2.17), relevant to describe the IPMC system in resonant condition, can be used for the measurement of the fluid's rheological parameters. In particular, although the equations (2.16) and (2.17) are applicable to all system's modes, the amplitude obtainable de-

creases with the order of the mode. For this reason, in the following the study of the system and the estimation of the parameters of the fluid will be done by using the processing of data relating to the first mode.

2.2. Experimental set-up

A measuring system, shown schematically in Figure 2.2, was realized for the experimental investigation of the prototypes, it allows to apply an electrical signal to the actuator and to measure the deflection obtained.

The study of the behavior expected also to the identification of the electromechanical model's parameters of the of the IPMC strip view as actuator, it means identify the system.

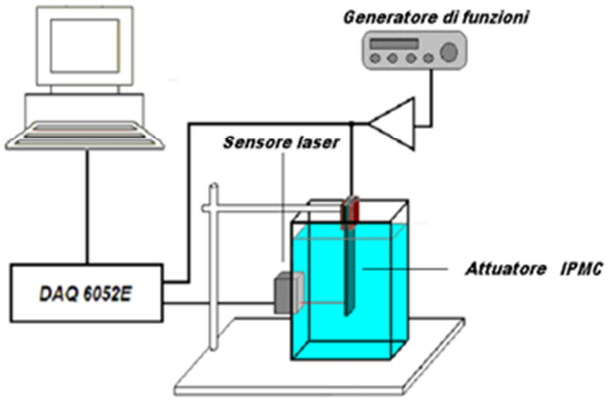

Figure 2.2: Measuring system realized for the experimental investigation

The signal is synthesized by a function generator and trought to a driver circuit, which has the purpose of providing adequate current to the actuator (which may even reach the hundreds of milliamps), is applied to a couple of elecrtrode that have the dual purpose of clamp and electrify the IPMC strip

For the realization of the circuit have been used two amplifiers:

- an OPA 547, in the configuration buffer, which has the purpose to supply the requested current to the membrane
- an INA 111 used to measure this current.

The measuring system also includes a laser distance sensor (Baumer Electric 12U6460/S35A), for detecting the deflection of the device in his free end point.

The signals were acquired by using a National Instruments data acquisition card (NIPCI_6052E).

Experiments were carried out using various test fluids, in particular distilled water and sucrose solutions with different concentrations of sucrose.

The choice fell on sucrose solutions because their rheological characteristics are known and easily available in the literature, also are solutions that have a significant relevance, from the application point of view, in biological field.

The procedure adopted for measure density and viscosity of the fluids is shown in Figure 2.3.

The system is put in vibrational motion, by applying a sinusoidal voltage input to the conditioning system, this signal has a constant amplitude and frequency linearly increasing with time.

Both the electrical stress and the signal provided by the distance sensor were collected in order to estimate the cantilever's frequency response.

The acquired data are then processed, by using a MATLAB® program, in order to estimate the value of the resonant frequency of the system and the quality factor Q. These parameters are then processed to estimate the values of viscosity and density.

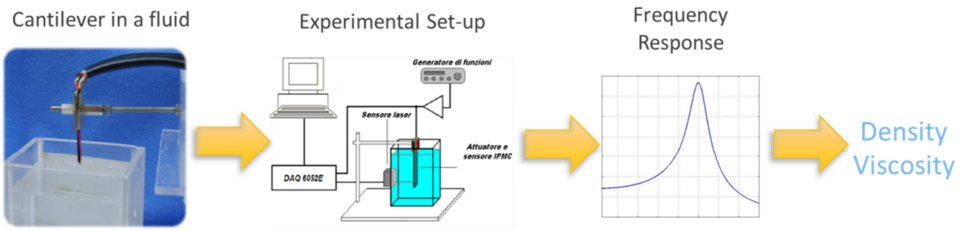

Figure 2.3: Procedure adopted for estimate the values of density and viscosity

2.3. First Version Results

In order to verify the operating principle of the viscometer, a set of measurements were performed by using sucrose solutions with different concentrations.

In particular, measurement campaigns were carried out by immersing the actuator IPMC in distilled water and sugar solutions with mass concentrations, normalized with respect to the condition of saturation, respectively equal to 0.3, 0.6 and saturated solution.

Figure 2.4 shows a comparison of the modules of the predicted frequency responses and the frequency responses obtained from data acquired.

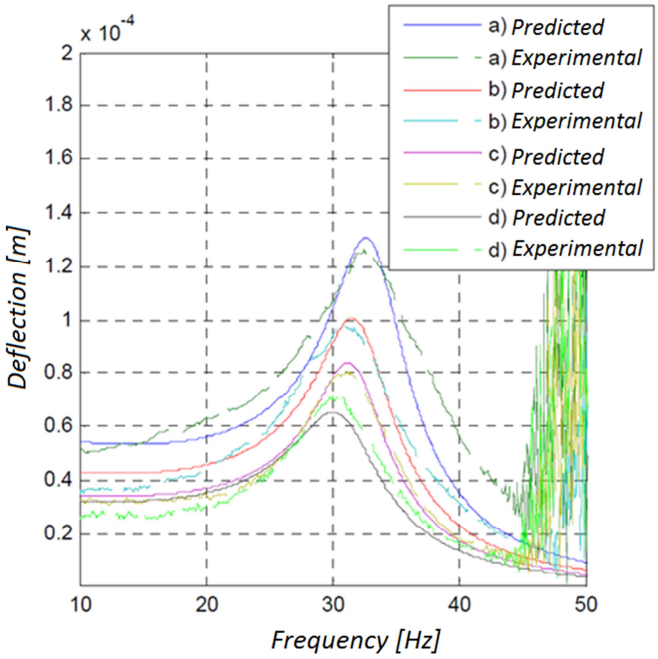

Figure 2.4: Module of the frequency response of the expected behavior and module of the frequency response of the first experimental version of the viscometer, immersed in solutions with different density values: a) distilled water, b) sugar solution 0.3, c) sugar solution and 0.6) saturated sugar solution.

As predicted by theory, the probe has a behavior related to the material that surrounds it.

From inspection of Figure 2.4 it is possible to note how the variation of both the values of the resonant frequency and the amplitude of the resonance peak, depending on the characteristics of the fluid in which the device is immersed.

In particular with the increasing of the concentration of sucrose in the solution, there is a corresponding lowering of the resonance frequency and a reduction of the value of the resonance peak.

Furthermore it is possible to assert that the processing of the data recorded by the measuring system has provided results in accordance with the estimates obtained from the analytical model previously reported.

Figure 2.5 and Figure 2.6 shows the experimental values of the resonance frequency for the first mode and the quality factor Q and the respective theoretical values, predicted at the computer by using algorithms based on the model previously described, in function of the solution's sucrose concentrations.

Also for these parameters the processing of experimental data has led to a good agreement between the estimates and the expected values from the models adopted.

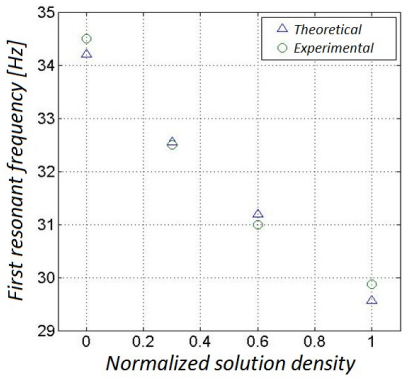

Figure 2.5: Experimental and predicted frequency response in differente sucrose solutions.

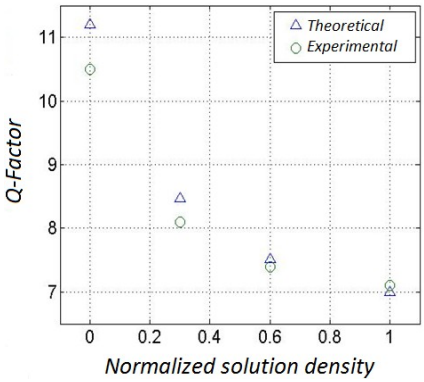

Figure 2.6: Experimental and predicted quality factor Q of the IPMC actuator in solution with different sugar concentrations.

3. The Second Version

The system described in the previous paragraph represents an intermediate prototype aimed at demonstrating the possibility to realize a viscometer using IPMC transducers. Nevertheless, that prototype was intended as a proof of concept and was of no practical application.
The first version lacked of an embedded sensor that would allow the measurement of the deformation of the vibrating actuator that allow to use the system in applications of real interest [36].

The device described in this section is, therefore, an evolution of the previous version, in fact, the laser distance sensor is replaced by a sensor IPMC [46].

The system is freed by external devices, such as the laser sensor to make the measurements, allowing the realization of a smart system, totally polymeric, able to provide directly an output signal, useful for the estimation of the rheological parameters of the fluid.

The sensing element of the proposed device is a multilayer beam realized superimposing an IPMC actuator and an IPMC sensor, as shown in Figure 2.7

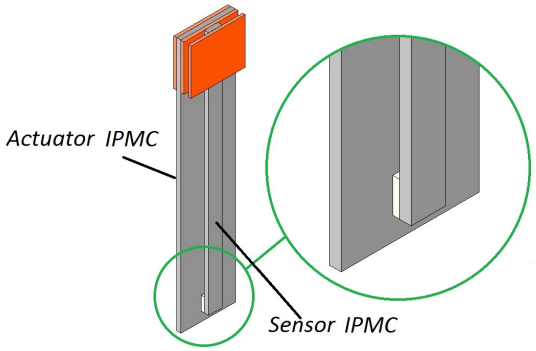

Figure 2.7: The sensing element of the proposed device

The two membranes are completely immersed in the fluid and placed in a cantilever beam configuration
The IPMC actuator is used to impose a vibration to the whole system, by applying to its electrodes an appropriate driver signal. The IPMC sensor is attached to the actuator so that it is forced to follow the system deflection. An electrical signal is, therefore, collected at the sensor electrodes and is used to measure the amplitude and the frequency of the deflection.

This signal is collected and processed to perform the measurement of the deflection, the laser is eliminated and is substituted by the IPMC sensing element, although it will still be used in order to have an independent measure necessary to validate the system.

As in the previous case, from this information it is possible to obtain the values of the system's resonant frequency and its quality factor and from these to trace the rheological characteristics of the fluid.

Obviously, in this second case, it is necessary to introduce in the model of the measuring system also the model of the sensor, as will be better specified in the following.

3.1. The model

Even for this version are valid are quantities expressed by the equation (2.16) and (2.17), but for this application, in which is used an IPMC sensor as sensitive element of the device, it is necessary to process the output signal of the sensor, which is presents as a short-circuit current, to retrive the deformation of the system.

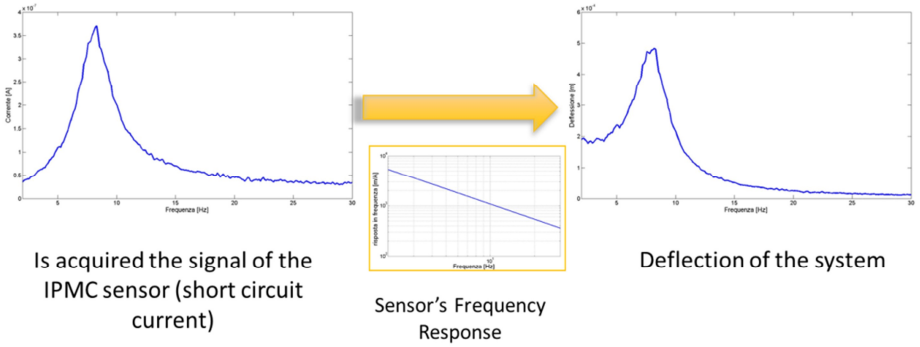

Figure 2.8: Conversion from the acquired signal to the real deflection

The model of the IPMC sensors has been previously described in the introduction chapter. In particular, the law which binds M_S, in the frequency domain, the deformation $\delta(s)$, setted to the free end of an IPMC sensor, and the corresponding short circuit current $i(s)$ is described by the following equation:

$$\boldsymbol{M_S = \frac{i(s)}{\delta(s)} = s\frac{3 \cdot d_s(s) \cdot t \cdot w \cdot Y}{4 \cdot L_S}} \tag{2.18}$$

where s is the Laplace operator, w is the sensor's width, t is the sensor's thickness, L_s is the point in which the deformation is applied (in this case the point of contact with the actuator), Y is the Young's modulus of the sensor, $d_s(s)$ is the electromechanical coupling term.

About the electromechanical coupling term, the function that gave the best modeling resulted in the following form [46]:

$$\boldsymbol{d_S}(\mathrm{s}) = \frac{\mathbf{k}}{(\mathbf{s}+\boldsymbol{\alpha})\cdot(\boldsymbol{s}+\boldsymbol{\beta})} \tag{2.19}$$

whose parameters were obtained in MATLAB through an algorithm of error minimization (see Appendix), the obtained parameters are reported in Table 2.1

Table 2.1: Values obtained for parameters characterizing the complex function d.

k (C s² N⁻¹)	α (Hz)	β (Hz)
-8.62 e-002	87,5	7.37 e+008

In Figure 2.9 and Figure 2.10 the experimental and simulated frequency response of the device considering the tip deflection and the output current of the IPMC sensor respectively are shown. As it can be noticed from the figures also in this new configuration the model is able to predict well the device behaviour.

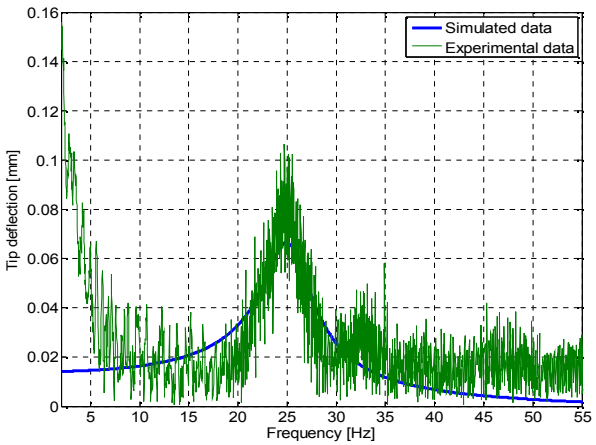

Figure 2.9: Experimental and predicted frequency response for the system, tip deflection in air.

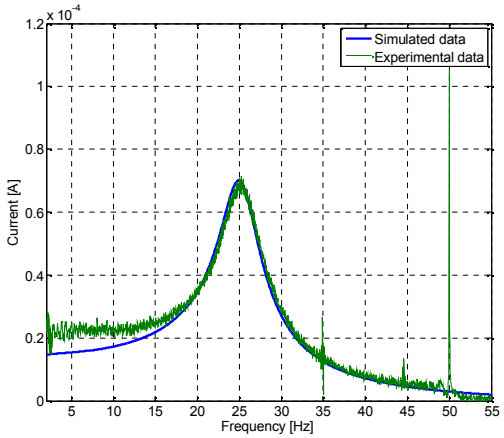

Figure 2.10: Experimental and predicted frequency response for the IPMC sensor output current in air.

In a similar manner to that described for the first prototype, the current produced by the sensor, is used to estimate the deformation of the vibrating system and from this the value of the resonance frequency of the first mode and this corresponding quality factor Q. From these values it goes back to the rheological parameters of the fluid by using the equations (2.16) and (2.17).

Figure 2.11 shows how the predicted frequency response well fit the experimental frequency response for the IPMC sensor output current in water.

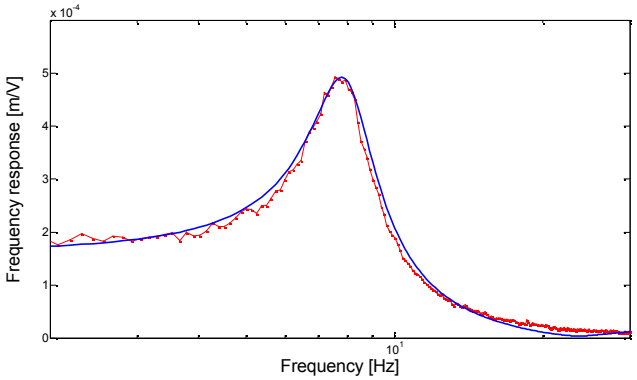

Figure 2.11: Experimental and predicted frequency response for the IPMC sensor output current in water.

3.2. Experimental set-up

The system adopted for the measurement of density and viscosity with this prototype is similar to the one used in the first version of the viscometer, the steps are shown Figure 2.12

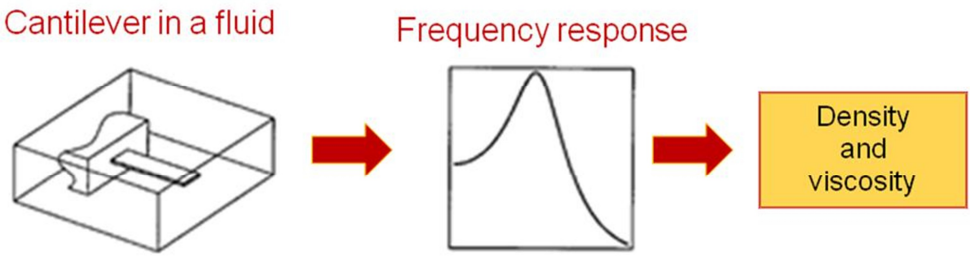

Figure 2.12: The steps of the adopted method for the measurement of density and viscosity.

As for the first analysis in a previous system (used to validate the theoretical approach), an IPMC based cantilever system was immersed in a fluid. It was forced by using a suitable signal and a vibrating motion was generated. The motion is produced by an IPMC actuator that is actuated with a sinusoidal swept input voltage.

The vibration of the system was detected by using the sensing IPMC element and a current was generated. Acquired data were processed in order to estimate the cantilever resonance frequency value, Q factor, and therefore the fluid rheological parameters.

Therefore this second version differs substantially from the previous for the addition of the IPMC sensor and the consequent presence of a current to voltage converter used as a conditioning circuit for the IPMC sensor, finally the system's deflection will then be a function of the obtained voltage. Even in this version is maintained the laser distance sensor (Baumer Electric 12U6460/S35A), but with the aim of allowing the independent measure of the deformation of the vibrating system.

Figure 2.13 shows an example of how the deflection derived from IPMC sensor signal well fit the real deformation of the vibrating system measured by the laser sensor

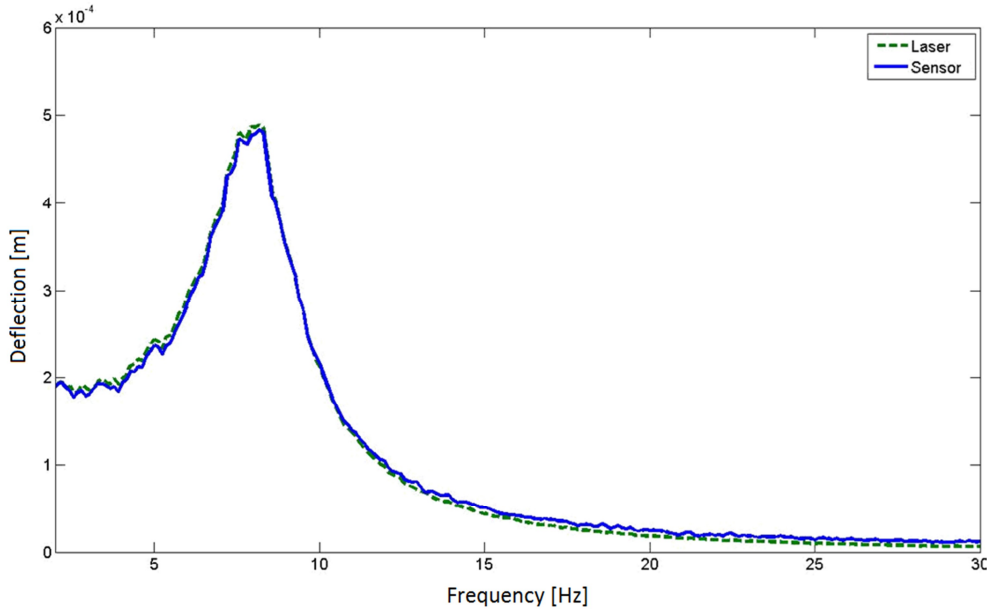

Figure 2.13: Comparison of the measure of the deformation of the vibrating system provided by the laser sensor with the deflection derived from IPMC sensor signal

The measurements were carried on using as testing fluids sugar solutions, as reported above.

The frequency response is measured and values of both viscosity and density of the fluid are derived. For the experiments a sample of IPMC *10* mm long, *3* mm wide was used.

3.3. Results

To perform the measurement campaign two membranes, as sensor and actuators, whose dimensions are shown in Table 2.2, have been used.

Table 2.2: Viscometer geometrical parameters

	Length	Width	Thickness
Sensor	22 mm	1, 5 mm	0, 180 mm
Actuator	23 mm	6, 0 mm	0, 180 mm

For each campaign 20 repeated measurements were performed.

In Figure 2.14 and Figure 2.15 the experimental and simulated frequency response of the device considering the tip deflection and the output current of the IPMC sensor are shown.

In particular in Figure 2.14 the points represent the single measures, the circles represent the average response and the continuous blue line represents the predicted response. This result has been achieved by immersing the device in deionized water.

The same schematization is true for Figure 2.15, that refers to the case when the device was immersed in a sucrose solution, 30% in mass.

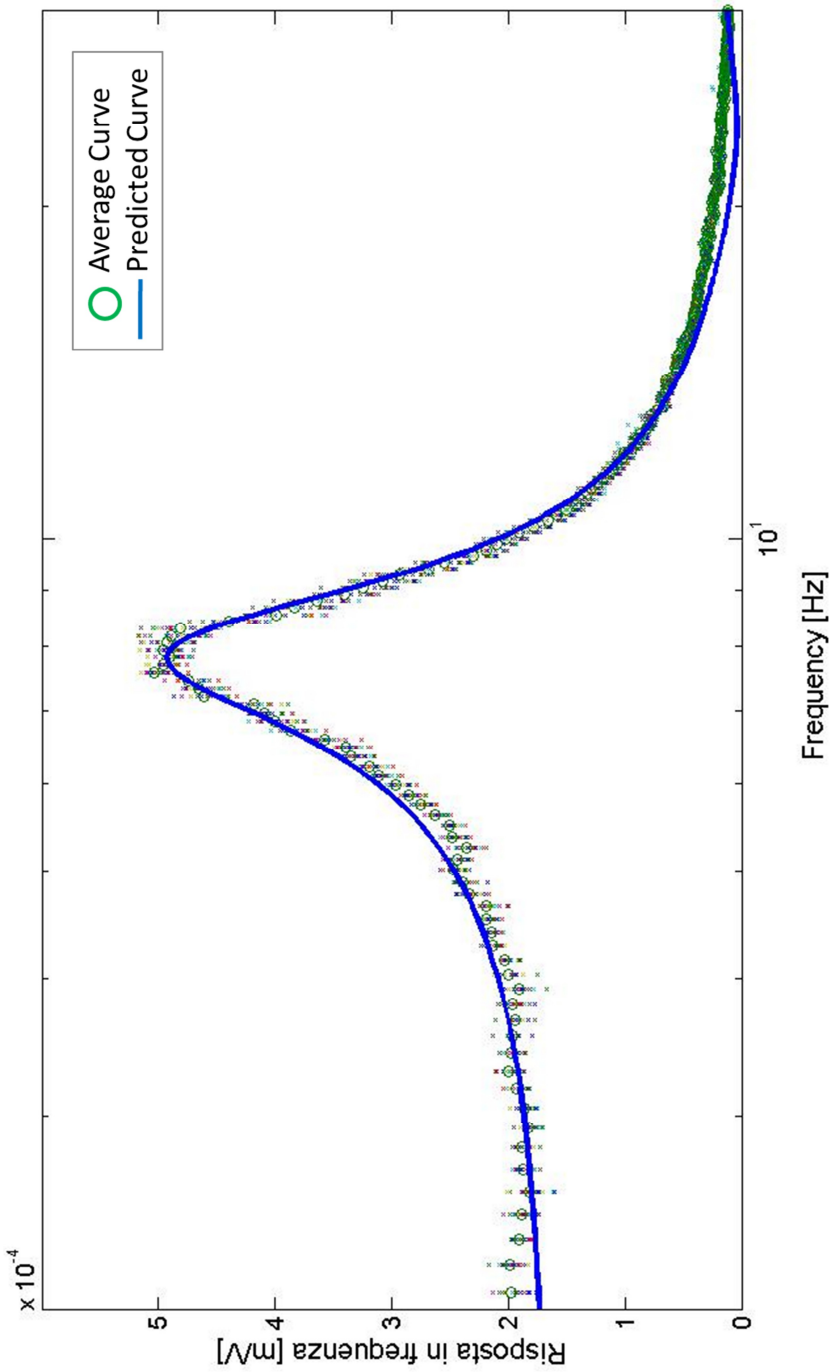

Figure 2.14: Experimental and predicted frequency response for the IPMC sensor output current in water

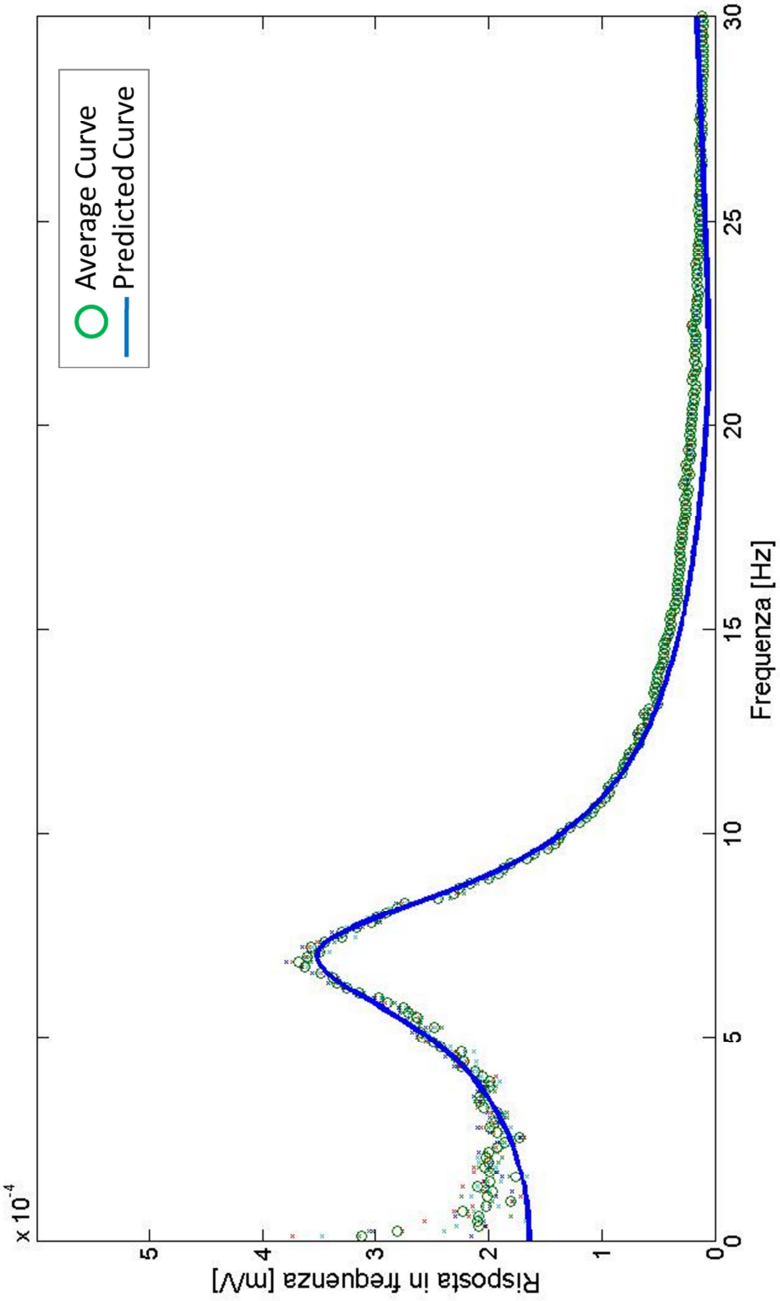

Figure 2.15: Experimental and predicted frequency response for the IPMC sensor output current in a sucrose solution 30% in mass

The model is able to predict well the behaviour of the system. The Table 2.3 shows some values of the rheological characteristics estimated using the proposed system and the corresponding values deduced from the literature.

Table 2.3: Experimental and theoretical density and viscosity values for different sucrose solutions

	ρ_f [Kg/m^3]		η [Pa s]	
	Experimental	*Theoretical*	*Experimental*	*Theoretical*
Deionized water	895.76	998	0.00091	0.001
0.3 sucrose solution	1031.7	1028	0.0022	0.0019
0.6 sucrose solution	1151.4	1134	0.0033	0.0031
saturated sucrose solution	1260.4	1282	0.0041	0.0044

4. Conclusions

The possibility to use IPMC transducers to realiza a viscometer has been described and experimentally investigated. The feasibility pf the proposed system has been verified for fluids with increasing densities and viscosities.The obtained results show the applicability of the proposed systems.

The system uses both acting and sensing IPMC to realize a smart system.

Chapter 3
SEISMIC SENSOR

1. Introduction

Ferrofluids (known also as magnetic fluids) are a special category of smart nanomaterials, in particular magnetically controllable nanofluids. These types of nanofluids are colloids of magnetic nanoparticles, such as Fe3O4, γ-Fe2O3, CoFe2O4, Co, Fe or Fe-C, stably dispersed in a carrier liquid [47], generally water or solvent, and covered with a thin polymeric layer, (surfactant) to prevent their agglomeration caused by Van der Waals forces [48]. These nanomaterials manifest simultaneously fluid and magnetic properties. A magnetic field applied to a ferrofluid volume exerts a magnetic force which causes the alignment of the ferrofluid particles in the direction of the field, modifying its physical properties such as density and viscosity. Moreover, under particular conditions, a ferrofluid volume subjected to a magnetic force can behave like a mass connected to tunable equivalent spring whose properties can be controlled by modulating the driving magnetic field [47]. Ferrofluids are widely used in sensors and actuators, where generally a small volume is used as the inertial mass, or in biomedical devices for diagnostic and therapy [49].

The need for smart sensors adapting their characteristics to the specific application is continuously emerging. Combining performances of IPMC sensors and magnetic fluid properties it is possible to optimize

the sensor performances in terms of its operating range, sensitivity and frequency response.

Here a seismic sensor exploiting both IPMC and ferrofluid is described [50].

The device consists of an IPMC beam housed in a small vial, filled with ferrofluid, whose properties depends on the magnitude of an external magnetic field applied to the device. This approach allows for the implementation of an active tuning of the sensor specifications (such as operating range, frequency behavior and responsivity) by an external magnetic field, which can be claimed as the main advantage of the proposed strategy.

In the following Sections, the sensing methodology developed, the description of the sensor prototype and the experimental set-up are presented, along with experimental results confirming the suitability of the proposed approach. Moreover, a possible form of device modeling is discussed in order to predict the relationship between main sensor features and the external magnetic field.

2. The realized system

2.1. The working principle

A schematization of the seismic sensor is sketched in Figure 3.1. The device consists of an IPMC Nafion® membrane used as the sensing element immersed in a ferrofluid. The membrane acts both as the seismic mass and the transducer that converts the imposed inertial stimulus into an electrical signal.

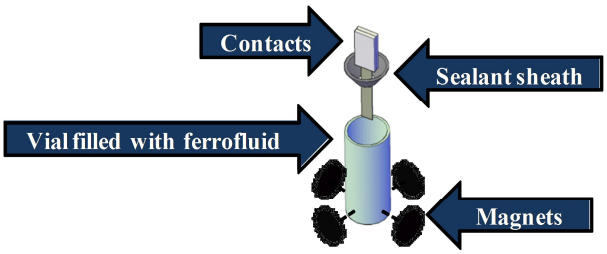

Figure 3.1: Schematization of the system.

The IPMC membrane is clamped, on the top side, by using electrified clamps, needed to collect the output short current.

The behavior of the IPMC membrane depends on both the density and the viscosity of the ferrofluid. The reason of choosing a magnetic fluid as the working fluid of the IPMC membrane is basically due to the intrinsic property of ferrofluid to change its characteristics (shape and density) as a function of an external magnetic field magnitude.

Actually, the idea behind the proposed sensor is the possibility to modify the sensor specifications by suitably tuning the strength of an external magnetic field applied to the device by a dedicated set of permanent magnets. The effect of the magnetic field amplitude will be twofold: it will influence the surrounding fluid distribution and the stiffness of the IPMC membrane soaked with ferrofluid. The first effect should reflect on the responsivity of the device: as the magnetic field increases the ferrofluid moves towards the vial walls and hence the density of the fluid surrounding the IPMC sensor will reduce thus increasing the responsivity of the device. Moreover, as the magnetic field increases the stiffness of the IPMC membrane will increase thus causing a shift of the resonance frequency of the device.

Summarizing, it can be affirmed that changes in the magnetic field strength (and consequently the ferrofluid shape and density) produces a modification in the sensor behavior both in terms of responsivity and frequency response (e.g. bandwidth), i.e. a smart sensing devices, with properties that can be modulated by the user has been obtained.

2.2. The real device

A first prototype of the system has been realized by using a IPMC strip 25 mm long by 4 mm wide. The membrane IPMC has been manufactured covering Nafion® 117 membrane (produced by DuPont®and distributed by Sigma-Aldrich®) with platinum deposed on both sides to form the electrodes. After Nafion® sheet surface treatment (or roughening), the electrodes deposition is performed through reduction in presence of dispersing agent (polyvinylpyrrolidone at concentration 0.001 M) both for primary and secondary plating.

The used Nafion® is about 180 µm thick, while electrodes are about 10 µm thick. This results in an IPMC sample that is about 200 µm thick, when wet. Table 3.1 summarizes some proprieties of Nafion®117.

The metallization on Nafion sheet is performed by using chemical procedures, such as ion exchange and reduction. The IPMC device has been realized by a customized manufacturing process implemented by our laboratory facility.

Table 3.1: Main proprieties of Nafion® 117

Proprieties	Value
Typical Thickness	*178 µm*
Basis Weight	*360 g/m²*
Density	*2.100 g/cm³*
Melting point	*350 °C*
Conductivity	*0.083 S/cm*

The membrane is sealed in a vial filled with EFH1 ferrofluid by Ferrotec [51]. A silicone sealing sufficed to avoid fluid leakage. The external magnetic field adopted to tune the fluid density is applied by a set of permanent magnets symmetrically positioned as respect to the IPMC sensor.

If subjected to a stimulus, the membrane oscillates and a current flows between the electrodes.

Such a current represents the output signal of the IPMC sensor; a current amplifier is used to amplify the current value and to transform it in a voltage value through a feedback resistance R (270 kΩ) [50].

2.3. The experimental results

The experimental set-up adopted to investigate the real behavior of the device is shown in Figure 3.2.

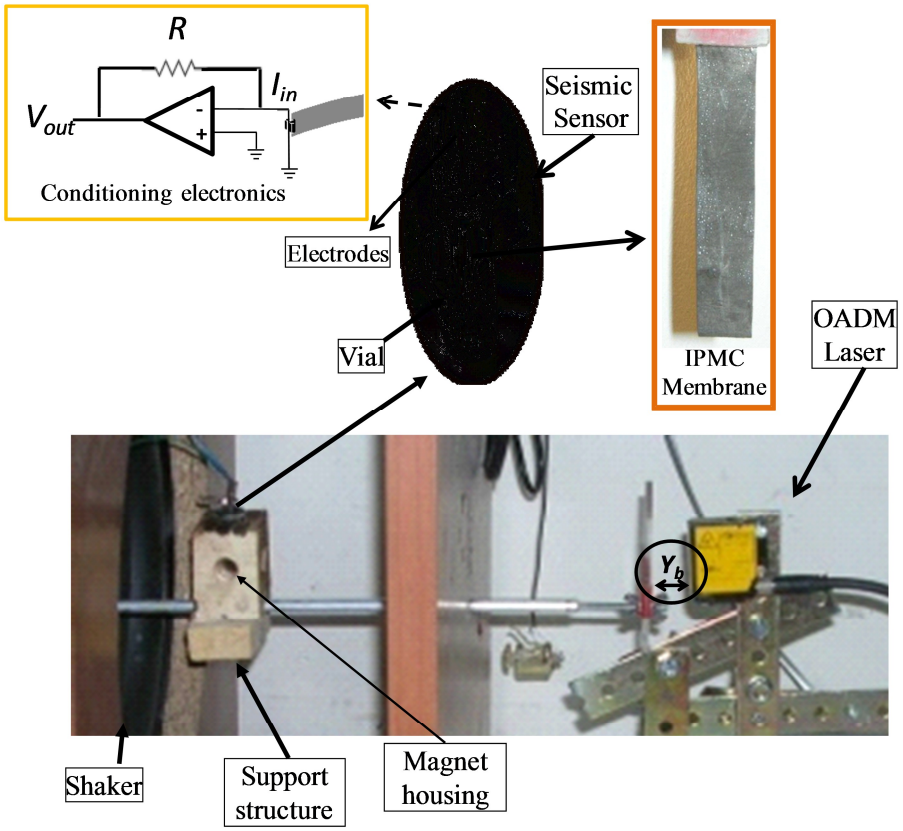

Figure 3.2: The experimental set-up.

The experimental set-up consists of a shaker used to stimulate a support structure where both the magnets and vial are placed. Moreover, the laser device, OADM 12U6460/S35A by the Baumer Electric®, is adopted to perform an independent measurement of the imposed inertial stimulus.

The IPMC-Ferrofluid seismic sensor is inserted in the vial. Moreover, through suitable electrodes the IPMC is connected to a conditioning electronics consisting of a I/V converter. In order to produce the desired magnetic field neodymium magnets are placed in suitable locations inside the support structure.

The shaker is driven by a sinusoidal sweep from 1 Hz to 100 Hz in a time interval of 30 s. Figure 3.3 shows both the electrical input to the shaker and the mechanical stimulus imposed to the seismic sensor, as recorded by the laser system.

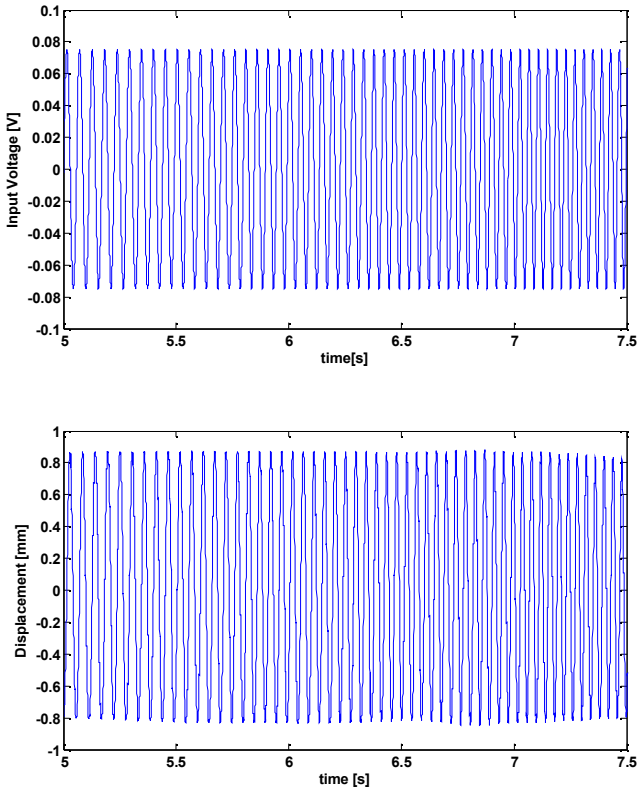

Figure 3.3: An example of the electrical input to the shaker (a) and the corresponding mechanical stimulus imposed to the seismic sensor recorded by the laser system (b).

The output voltage V_{out} is acquired by a data acquisition board (DAQ PCI 6052E) and a dedicated interface developed in the Labview® environment. Acquired signals are then conveniently processed and converted in the current domain.

In order to test the system behavior for different values of the applied magnetic field, H_{ext}, different set of permanent magnets are used. In particular, the magnetic field distribution along the vial walls has been maintained as much uniform as possible.

The system behaviors (frequency response) in different operating conditions are reported in Figure 3.4

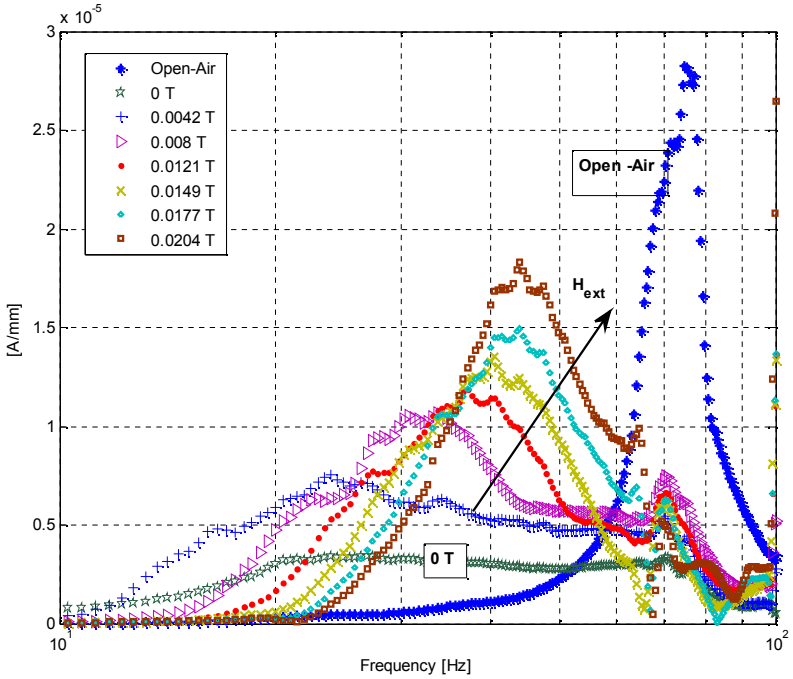

Figure 3.4: Frequency response of the seismic sensor for different working conditions: sensor in open-air; immerse in ferrofluid for different values of H_{ext} [0 T, 0.0042 T, 0.008 T, 0.0121 T, 0.0149 T, 0.0177 T and 0.0204 T]. Figure labels highlight the case in open-air, H_{ext}=0 T, while the arrow shows the device behavior for increasing value of H_{ext}.

Values of the magnetic field experienced by the IPMC membrane were measured independently through a Hall Effect sensor **(**SS413A by Honeywell) which has been suitably placed in the membrane position inside the vial.

In particular, the sensor response when operated in open-air (without ferrofluid) and when immersed in ferrofluid for different values of H_{ext} [0 T, 0.0042 T, 0.008 T, 0.0121 T, 0.0149 T, 0.0177 T and 0.0204 T] are shown. Data reported have been obtained averaging over 20 acquisitions. Dispersion between the 20 observations estimated as the maximum of the standard deviations (σ) over inspected frequency values has been also computed. As it can be observed, the device response is strictly

influenced by the presence of the external magnetic field and as expected for increasing values of the magnetic field (and hence of the ferrofluid density influencing the membrane stiffness) the resonant frequency of the device increases. Moreover, the device responsivity increases when H_{ext} increases due to the ferrofluid re-distribution on the vial walls which will modify the density of the fluid surrounding the IPMC membrane.

It can be observed that the IPMC beam immersed in the ferrofluid shows a decrease of its responsivity and its resonance frequency with respect to the IPMC working in open air.

Table 3.2 reports the obtained resonance frequency, the responsivity, the resolution and the estimated σ value as function of the applied magnetic field.

As evincible from the obtained results, the effect of magnetic field on the device resonant frequency seems to be negligible since 0.0177 T. This effect can be justified by a saturation effect on the membrane stiffness variation by H_{ext}.

Table 3.2: sensor specificatons as a function of the applied magnetic field, H_{ext}

Magnetic field [T]	Resonant Frequency [Hz]	Responsivity [A/mm]	Resolution [mm]	σ [A]
0.0042	*23.93*	*5.08e-6*	*0.038*	*1.93e-7*
0.008	*33.69*	*6.00e-6*	*0.069*	*4.14e-7*
0.0121	*37.11*	*9.35e-6*	*0.39*	*3.64e-6*
0.0149	*40.53*	*1.20e-5*	*0.029*	*3.48e-7*
0.0177	*43.95*	*1.43e-5*	*0.021*	*3.00e-7*
0.0204	*43.95*	*1.77e-5*	*0.016*	*2.83e-7*

3. The Device Modeling

The seismic sensor has been modeled as a distributed system by using the equation of a beam pinned by one end, and subjected to vibration motion [52]. Assuming that the deflection is small enough to avoid a deformation in the lateral walls of the element *'dx'*, the equilibrium forces equation is written as:

$$\rho A \frac{\partial^2 u(x,t)}{\partial t^2} + YI \frac{\partial^4 u(x,t)}{\partial x^4} + BI \frac{\partial^5 u(x,t)}{\partial x^4 \partial t} + \beta \frac{\partial u(x,t)}{\partial t} = f(x,t) \tag{3.1}$$

where $u(x, t)$ is the deflection of the beam, ρ is the mass density, A is the transversal section of the pinned IPMC which has a rectangular shape, Y is the Young's modulus of the IPMC membrane, which has been assumed to be constant in the considered frequency range (0.6 GPa) and I is the area moment of inertia. The $f(x, t)$ is the forcing term of the beam. The internal and external frictions have been modeled by parameters B and β, which take into account for the effect of H_{ext} on the beam stiffness and the rheological characteristics of the surrounding fluid, respectively.

From solution of Eq. (3.1) the sensor response, relating the displacement, Y_b (see Figure 3.2), with the short circuit current, i_{sc}, can be expressed as [52]:

$$\frac{i_{sc}(s)}{Y_b(s)} = s^3 M_v^{\star}(s) \frac{\mathrm{k}}{L_t} \frac{\int_0^{L_t} W_1(x)}{s^2 + 2\xi\omega_{\mathrm{n}} s + \omega_{\mathrm{n}}^2} \left(\frac{\partial W_1(x)}{\partial x}\right)_{x=L_t}. \tag{3.2}$$

where:

ω_n and ξ depend on parameters B and β,

$W_1(x)$ is the first mode shape function,

k is the gain,

$L_t = 17mm$ is the membrane length (without considering the clamping part),

$M_v^*(s)$ is given by:

$$M_v^*(s) = wd(s)\mathrm{Y}\frac{h}{2} \tag{3.3}$$

where w and h are the width and thickness of the rectangular membrane section, while *d(s)* is given by:

$$d(s) = \frac{\prod_{i=1,n}(s-Z_i)}{\prod_{j=1,m}(s-P_j)} \tag{3.4}$$

where Z_i and P_i are zeros ans poles values of function *d(s)*.

Equation (3.2) is used to model the sensors behavior in open-air and immersed in ferrofluid subjected to different applied magnetic field. To such aim model (3.2) has been fitted on experimental data shown in Figure 3.4 by using a minimization procedure [53].

As first, model (3.2)-(3.4) has been estimated in the case of open-air operation obtaining parameters shown in Table 3.3 and Table 3.4.

Table 3.3: Parameters estimated *D(S)* for open Air operation

$Z_1(s^{-1})$	$P_1(s^{-1})$	$P_2(s^{-1})$	$P_3(s^{-1})$
-72.34	-749.63	-82.166	-20.34

Since part (3.3) of model (3.2) is strictly related to the IPMC operation in air, it will be mantained while minimizing model (3.2) for other operating conditions.

Model parameters identified for the whole set of considered operating conditions are reported in Table 3.4. The sensing system response is ruled by changes in the damping coefficient and natural frequency values coherently with the expected behaviour of the device.

Table 3.4: Model parameters estimated for different operating conditions of the seismic sensor

Operating conditions	ξ	ω_n (rad/s)	k
0 T	0.414	135.873	2.639e-07
0.0042 T	0.291	139.286	4.330e-07
0.008 T	0.180	195.564	3.962e-07
0.0121 T	0.170	223.251	4.215e-07
0.0149 T	0.169	239.251	4.719e-07
0.0177 T	0.160	262.251	4.845e-07
0.0204 T	0.150	266.491	5.767e-07
Open-Air	0.044	467.745	2.951e-07

The comparison between the observed frequency responses of the device and trends predicted by above mentioned models are shown in Figure 3.5 and Figure 3.6.

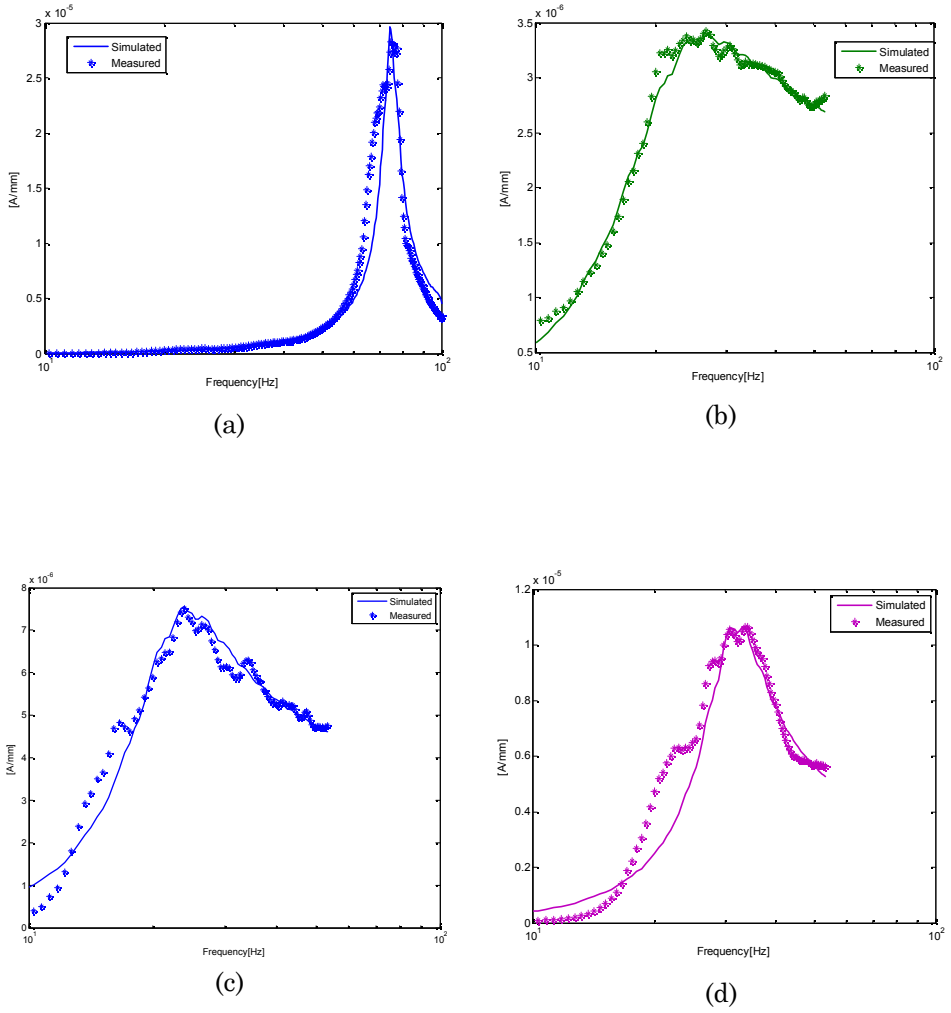

Figure 3.5: Frequency response of the seismic sensor in open-air (a); immerse in ferrofluid and subjected to a magnetic field of 0 T (b), 0.0042 T (c), 0.008 T (d)

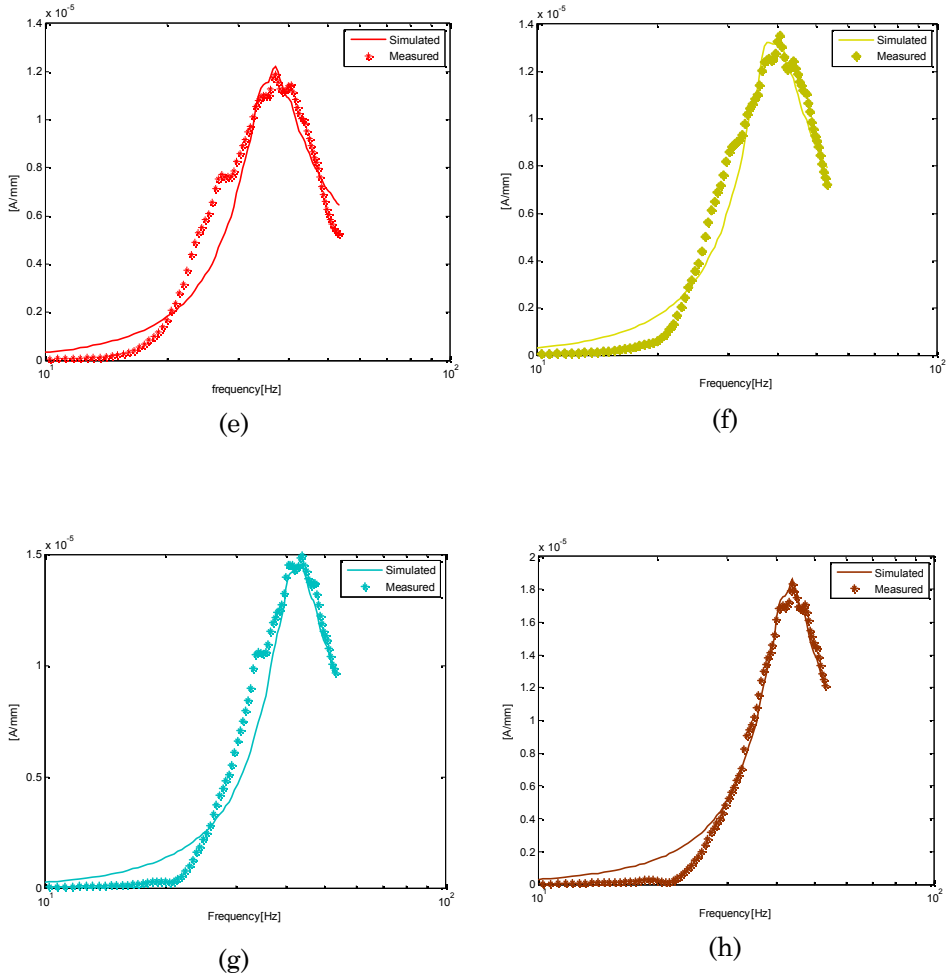

Figure 3.6: Frequency response of the seismic sensor immerse in ferrofluid and subjected to a magnetic field of 0.0121 T (e), 0.0149 T (f), 0.0177 T (g) and 0.0204 T (h).

The following performance index has been used to assess the model fitting:

$$J = 100 \cdot \frac{\sqrt{\sum_i \left(M_I^{\,measured} - M_I^{\,simulated} \right)_i^2}}{\sqrt{\sum_i \left(M_I^{\,measured} \right)_i^2}} \qquad (3.5)$$

where $M_I^{\,measured}$ is the measured sensor frequency response while $M_I^{\,simulated}$ is the predicted one.

Values of J, reported in Table 3.5, confirm the suitability of models adopted to predict the behaviour of the proposed seismic sensor.

Table 3.5: index J adopted to asses the model performances

0 T	0.0042 T	0.008 T	0.0121 T	0.0149 T	0.0177 T	0.0204 T	Open Air
4.85%	6.90%	13.72%	14.61%	15.14%	12.75%	7.37%	15.18%

4. Conclusions

A seismic sensor based on the interaction between a Ionic Polymer Metal Composite and a ferrofluid was presented. The system allows to purposefully tune the sensor behavior (e.g. operating range, frequency bandwidth and responsivity) by using a magnetic field. Though, applications exist where the seismic sensor is intended as an ad-hoc device required to measure vibration with established characteristics, working conditions can be envisaged where the required sensor specifications need to be changed according to the mechanical solicitation or the application scenario.

Experimental results demonstrate that the sensor behavior depends on the fluid density and its specifications can be tuned by an external magnetic field.

The possibility to implement an active tuning of the sensor specifications (such as frequency behavior and responsivity) by an external

magnetic field is the main advantage of the proposed strategy and represent an example of smart sensing device based on EAPs.

Chapter 4
POWER HARVESTING

1. Introduction

EAPs have the ability to deliver an electrical signal in response to mechanical stress. This reaction can be used to scavenge power from ambient vibration sources. The power harvesting properties of a new class of all polymeric ionic electroactive materials (IP^2Cs) from vibrating sources have been introduced, experimentally investigated and compared with corresponding harvesting properties of IPMC.

Moreover, IP^2C could be suitable for the realization of wireless sensor networks with applications relevant in the fields mentioned above.

One of the main problems with wireless sensor networks is powering and a lot of studies have been carried on to investigate the possibility to scavenge energy from environment [54].

One of the main source of energy considered for power harvesting is mechanical vibration.

Studies on the harvesting capabilities of ionic polymer-metal composites (IPMCs) from mechanical vibration have been published. The power harvesting properties of IPMCs in air, because of base mechanical excitation, are reported in [55]. The power harvesting properties of IPMC in water have been investigated in [56].

Here the energy harvesting capabilities of IP^2C in air are described.

2. Investigation of IP²C Energy Harvesting properties

The power harvesting properties of IP²Cs and the corresponding performance obtained by using IPMC transducers, which can be considered as a parent technology, are investigated in the following.
Results reported show that IP²C have energy harvesting capabilities and could represent a suitable technology to power sensors and even to realize all polymeric post-silicon wireless sensor networks

2.1. Characteristics of the used transducers

Transducers based on Nafion®117 (produced by Dupont® and distributed by Sigma-Aldrich Group) as the ionomer membrane have been considered.

If water is used as solvent for IPMCs or IP²Cs, they experience water loss that causes several limitations in terms of performance and applications. In fact, the applied electric potential must be limited to less than 1.3 V at room temperature, to avoid electrolysis and water evaporation in open air. Moreover, organic electrodes can degrade during sample hydration in the solvent.

These problems can be overcome by using solvents other than water. For example, ethylene glycol (EG) which, like water, consists of polar molecules, or 1-ethyl-3-methylimidazolium trifluoromethanesulfonate (EmI-Tf), which is an ionic liquid (IL), existing as liquid at room temperature and showing high inherent stability [57], have been proposed for the case of IPMCs and will be taken into account here for IP²Cs.

By substituting the water in the IP²Cs with EG or an IL it is therefore possible to obtain all-organic devices with low manufacturing costs, to overcome the dehydration problem and to improve the electrical performance because of the enhancement of the electrical conductivity of the PEDOT:PSS used as electrode.

In order to Compare various types of transducers (IPMC and IP²Cs) ethylene glycol (EG) and 1-ethyl-3-methylimidazolium trifluoromethanesulfonate (EmI-Tf) were used as the solvents and poly(3, 4-

ethylenedioxythiophene)–poly (styrenesulfonate) (PEDOT:PSS - Baytron® P HC V4) as the conducting polymer.

In particular, regarding the solvents, ethylene glycol viscosity is about 16 times higher than that of water at room temperature, and has a greater molecular weight. It is used as an anti-freeze.
Like water, it consists of polar molecules and has already been suggested to be used as a solvent for IPMC [8]. In Table 4.1 some chemical properties of EG are reported [58].

Table 4.1: Some properties of ethylene glycol

Properties		Structure
Relative density	1.109 g ml^{-1}	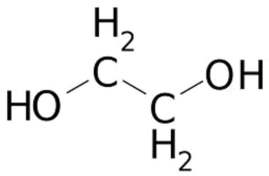
Molecular weight	62.07 g mol^{-1}	
Boiling point	197.6 °C	
Water solubility at 17.5 °C	10g/100 ml	
Melting point	−13 °C	
Dielectric constant at 20 °C	41.4	
Viscosity at 25 °C	16.1 × 10−3 Pa s	

EmI-Tf belongs to the class of ionic liquids: they are salts containing only charged species that exist in their liquid state at room temperature. They have immeasurably low vapor pressures, electrochemical stability windows of 4.0 V or more, and are thermally stable to temperatures as high as 400 °C. Furthermore, ionic liquids have high ionic conductivities and can be used as electrolytes for a variety of applications, including electrochemical capacitors [59] and conducting polymer actuators [60].

The ionic liquids can be used as solvents for Nafion transducers for their stability and, therefore, to avoid the problem of solvent evaporation. Also, the ionic liquids are ionically conductive and should therefore facilitate ionic motion in the Nafion® membrane. EmI-Tf has a viscosity of $35\times10^{-3} – 45\times10^{-3}$ Pa•s, at 25 °C. The structure and more relevant properties of EmI-Tf are reported in Table 4.2 [61].

Table 4.2: Some properties of EmI-Tf

Properties		Structure
Relative density	1.387 g ml^{-1}	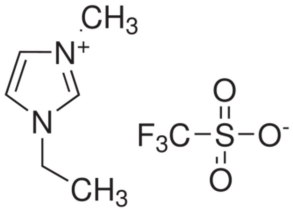
Molecular weight	260.23 g mol^{-1}	
Boiling point	>350 °C	
Water solubility at 17.5 °C	Fully soluble	
Melting point	−9 °C	
Ionic conductivity	8.6–9.3 mS cm^{-1}	
Electrochemical stability window	4.1 V	

The organic conductor poly(3, 4-ethylenedioxythiophene)–poly(styrenesulfonate) (PEDOT:PSS) and in particular the Clevios™ P HC V4 was used, because it is one of the best known conducting polymers: it shows excellent electrical conductivity as well as processability. The conductivity value is 200 S cm^{-1}, as reported in [62].

2.2. Experimental set-up

An experimental set-up was realized to evaluate the power generated by the membranes able to provide the mechanical stimulus and to collect the electrical signals, generated by membrane. Data were acquired and processed, in order to estimate the power spectral density.

The experimental set-up, adopted to measure the power generated from the membranes, is shown in Figure 4.1.

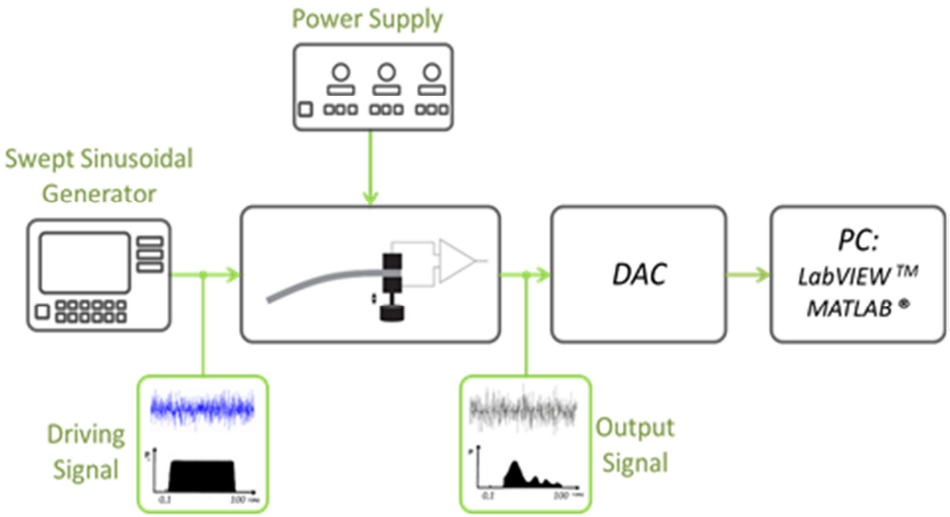

Figure 4.1: Experimental set-up

Samples of both IPMCs and IP²Cs were realized and mounted horizontally in cantilever beam configuration on a shaker (Tira TV 50009) by using a couple of copper electrodes realized on a printed board.

A waveform generator drives the vibration system to impose the mechanical oscillation to the fixed end point of the membrane and to obtain the base vibration, i.e. the mechanical source for power harvesting.

The signals obtained in response to mechanical excitation (short-circuit current or open circuit voltage are required for the estimation of the harvested power), after being processed by the conditioning circuits specially designed, are acquired by using a National Instruments PCI-6052E acquisition card. The vibration imposed to the base of the transducer was detected by using a laser distance sensor (model: Baumer OADM 12U6460/S35A).

The characteristics of the transducers used for the measurement surveys are reported in Table 4.3.

Table 4.3: Characteristics of Used Transducer

Code	Type	Electrode	Solvent	Length (mm)	Free Length (mm)	Width (mm)	Thickness (mm)
EG6	IP²C	PHCV4	Glicole Etilene	21	17	4	0.2
EMI2	IP²C	PHCV4	EmI-Tf	21	17	4	0.2
W3	IP²C	PHCV4	Water	21	17	4	0.2
W4	IPMC	Platino	Water	21	17	4	0.2

More specifically, the parameter **Length** refers to the total length of the transducers, while the parameter **Free length** refers to the part of the transducer that is not fixed under the rigid copper electrodes. The parameter **Thickness** has been estimated by taking into account the typical thicknesses of both nafion and of the electrodes. The parameter **Solvent** refers to the type of solvent contained inside of the membrane.

The mechanical excitation consists for all experiments of a swept sinusoidal displacement, with frequency in the range 0.1 Hz to 100.0 Hz, duration 60.0 s, and amplitude of the base motion of about 1.0 mm (the motion is recorded by the laser sensor).

A top view of the shaker, a mounted Device Under Test (DUT) and the laser sensor is seen in Figure 4.2.

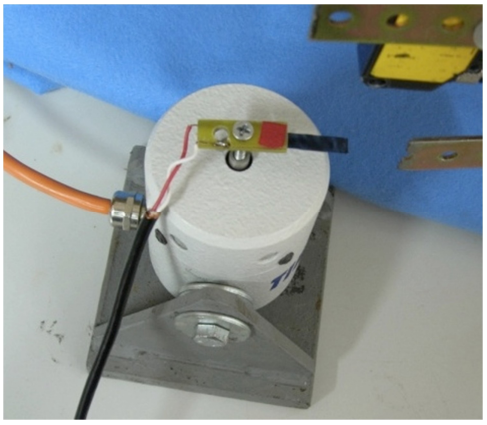

Figure 4.2: The mechanical part of the set-up used to investigate the power harvesting capabilitiers of polymeric transducers. The laser sensor is used to measure the base vibration of the DUTs.

2.3. Results

Twenty acquisitions have been performed for each sample and the corresponding mean power, as a function of the frequency of the imposed deformation has been estimated. As an example in Figure 4.3, Figure 4.4 and Figure 4.5 zooms in time domain of the deformation imposed by the shaker, as recorded by the laser sensor, of the short circuit current, and of the open circuit voltage are reported, respectively.

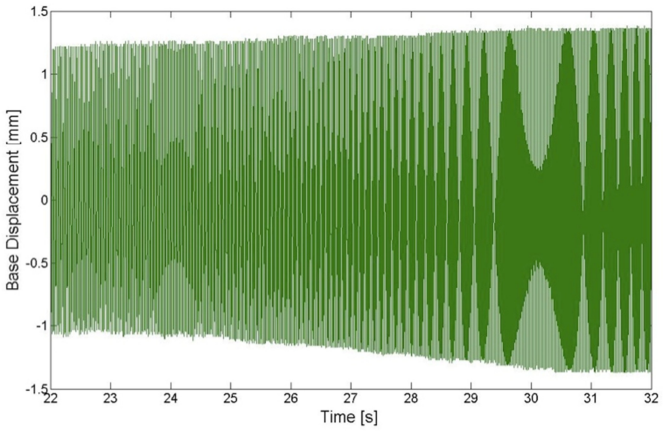

Figure 4.3: An example of the DUT base displacement imposed by the shaker and recorded by the laser sensor.

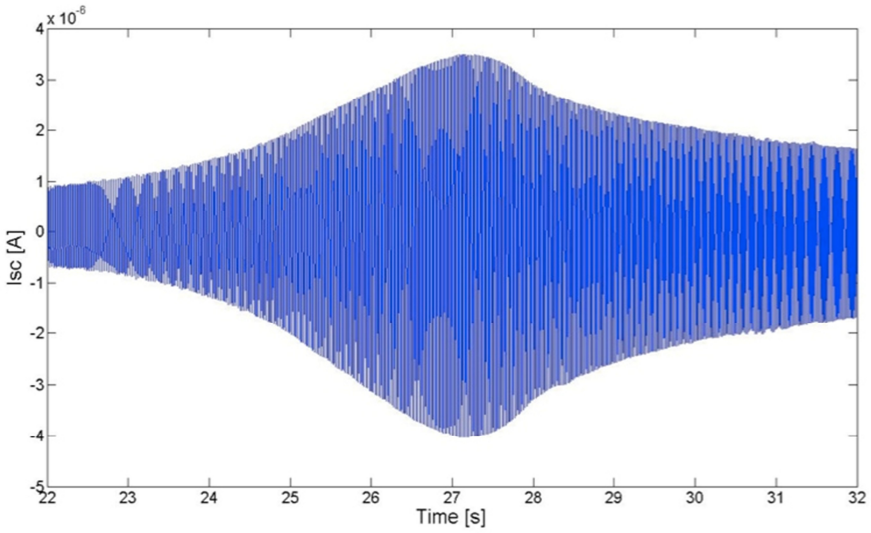

Figure 4.4: An example of the short circuit current produced by a polymeric transducer (IPMC) as a reaction to the base displacement shown in Figure 4.3

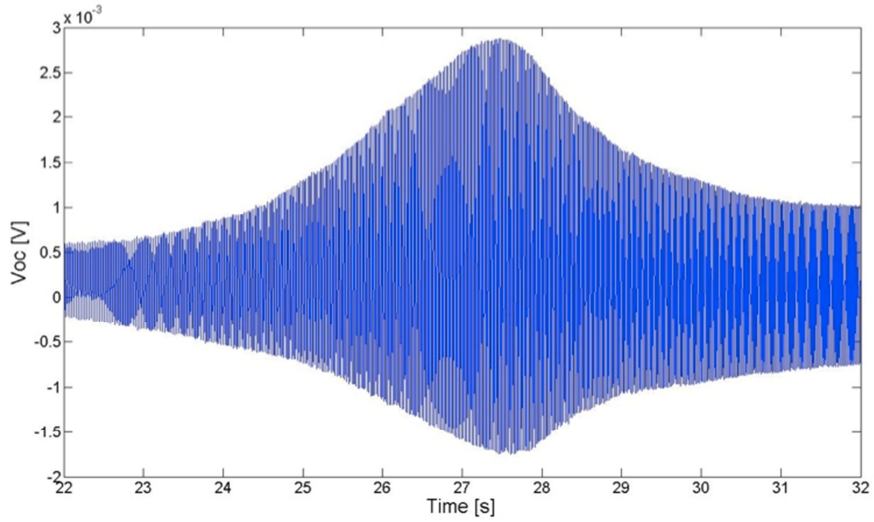

Figure 4.5: An example of the open circuit voltage produced by the polymeric transducer considered as a reaction to the base displacement shown in Figure 4.3

Figure 4.6 shows the frequency domain representation of the short circuit current $I_{sc}(j\omega)$, reported in logarithmic scale, for the IPMC and the IP²C samples under investigation. It is possible to observe that the IP²C short circuit current, in the investigated frequency range, is larger than the corresponding current produced by the IPMC sample.

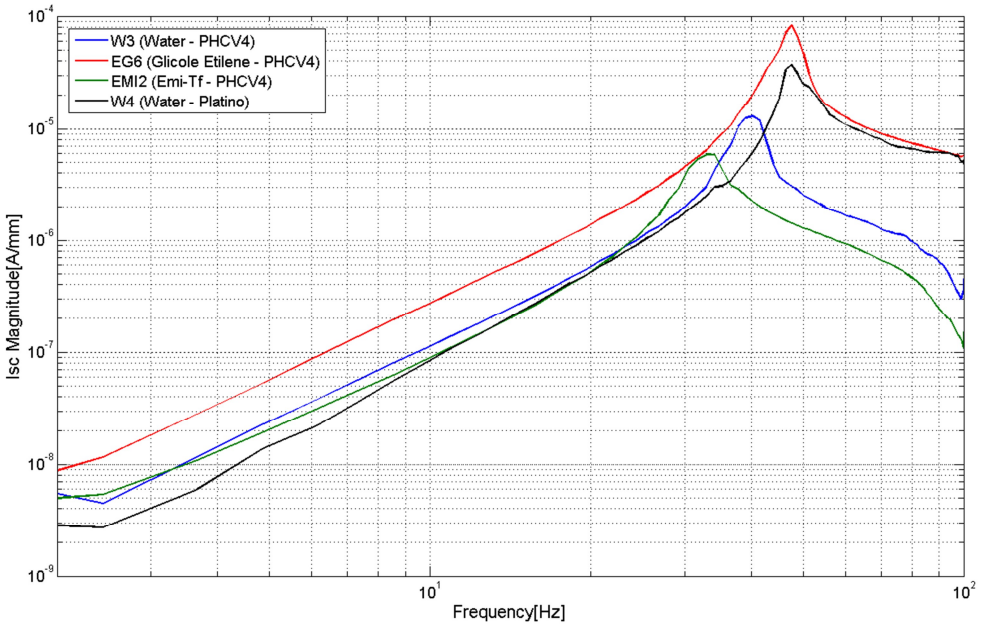

Figure 4.6: Comparison in the frequency domain of the short circuit current for an applied base vibration produced by the IPMC and IP²C samples.

Figure 4.7 shows the frequency domain representation of the open circuit voltage $V_{sc}(j\omega)$ for the IPMC and the IP²C samples under investigation. It is possible to observe that also the IP²C open circuit voltage is larger than the corresponding quantity produced by the IPMC sample .

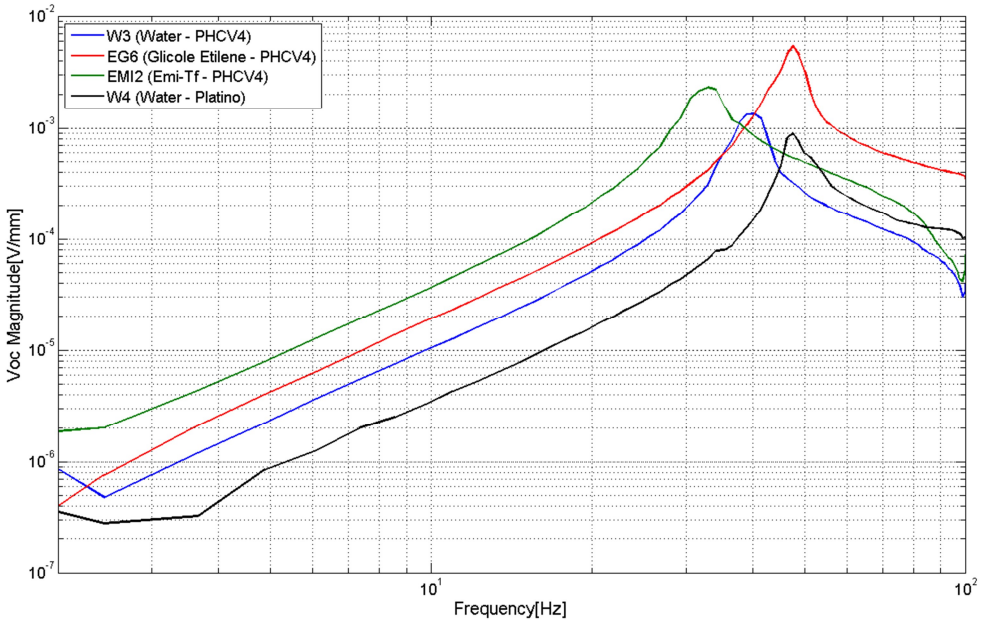

Figure 4.7: Comparison of the frequency domain representation of the open circuit voltage for an applied base vibration produced by IPMC and IP²C samples.

Data on short circuit current and open circuit voltage have been therefore used to estimate the available power, as indicated by (4.1).

All the data acquired was used to calculate the power generated by the devices. Such quantities allows, in fact, to estimate the maximum available power $P(s)$, in the frequency domain, as [55]:

$$P(s) = \frac{|V_{oc}(s)||I_{sc}(s)|}{8} \tag{4.1}$$

where:

- $V_{oc}(s)$ is the open circuit voltage
- $I_{sc}(s)$ is the short circuit current, produced because of the base vibration

and an adapted load is supposed.

The available power estimation in seen in Figure 4.8 for the IPMC and IP²C transducers under investigation.

It is possible to observe that, because of the produced short circuit current and open circuit voltage values, the IP²C in the investigated frequency range over performs the IPMC as a mechanical vibration power harvester. Such superiority is larger in the proximity of the IP²C resonance frequency.

For a better comparison of the devices performances the obtained values of maximum short circuit current, open circuit voltage, and available power, as estimated at the resonance frequency, are reported in Table 4.4 for the DUTs.

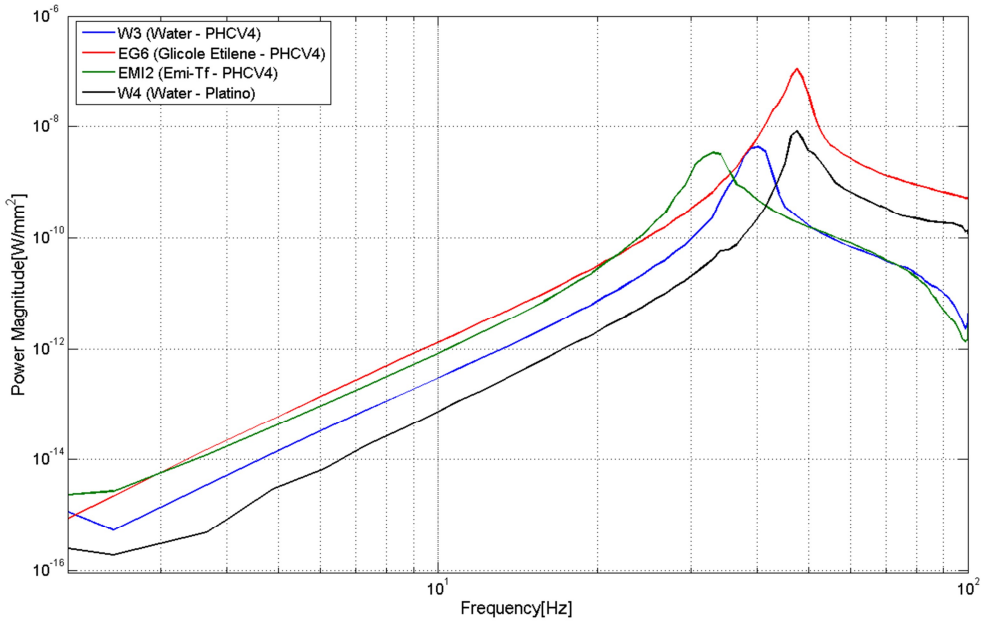

Figure 4.8: Comparison of the available mean power for an applied base vibration produced by the investigated samples

From the analysis of results reported in Table 4.4 it is possible to observe that the resonance frequency of the two transducers it quite the same, regardless of the change in the nature of the electrodes and of the solvent.

Table 4.4: Measured Electrical Quantities

Sample	Resonance frequency [Hz]	Isc_{max} [μA/mm]	Voc_{max} [mV/mm]	$Pout_{max}$ [μW/cm²]
EG6	47, 6	82, 76	5, 43	5.616
EMI2	33	5, 80	2, 32	0.171
W3	40	12, 88	1, 34	0.216
W4	47	37, 17	0, 89	0.4154

Also, as it regards the short circuit current the IP²C produced a maximum value that is about two times larger than the corresponding value produced by the IPMC.

For the case of the open circuit voltage the IP²C gives again a value larger than the IPMC. More specifically, a maximum voltage value that is about 6 times larger was given by the IP²C.

The results reported have shown the superiority of the IP²C that uses Clevios™ P HC V4 and EG as solvent, over IPMC as a power harvester. In fact, the value of the power available for the IP²C, if matched load conditions are supposed, is about 13, 5 larger than the maximum value estimated for the IPMC.

3. Bi-Stable Power Scavenger

Analysis of the IPMC and IP²C behaviour as power harvester, described in the previous section, has shown that these transducers are able to supply a signal which, although small in amplitude, may be used in the future to harvest energy from environmental noise.

One of the main limits of the first version was the small bandwidth in which the devices shows a response.

In fact the bandwidth for all the samples were smaller than 20 Hz. Considering this, it will be necessary to tune the size of the cantilevers in function of the vibrations that we aspect to find in the environment.

Due to this limit could be easy to lose an important part of the harmonic components that constitute the environmental noise.

A typical non linear inertial power generator employs a mass suspended within a frame that performs work against a damping transduction force as it moves relative to the frame [63] [64].

Due to of its mechanical characteristics this system thus realized has two states of equilibrium. This type of generator performs optimally when it is able to perform transitions between the equilibrium states

However, three problems prevent this approach from being applied to low-frequency vibrations:

1) as the frequency drops so does the expected power density
2) most low-frequency vibrations are caused by environmental sources and are not periodic
3) the vibrations may haven't the characteristics necessary to allow the passage from one stable state to another.

Here the design, fabrication, and testing of an inertial micro power scavenger that utilizes the bistable motion of a mechanical mass to convert ambient vibrations into electrical output energy is described. The generator incorporates an IPMC strip to initiate mechanical oscillations in an electromagnetic scavenger.

In the following sections will be shown how the use of a bistable configuration will increase both bandwidth and amplitude of the electrical signal produced.

3.1. Prototype Development

A prototype was fabricated and assembled to test out the proposed architecture. A support structure were realized with the aim to transfer the mechanical stress to the electroactive part of the harvesting system.

Electrodes specially designed were made with the dual purpose of clamp the IPMC strip and collect the signal produced from it.

The electrodes were rigidly anchored to a shaker through a structure in plexiglass and two common standoffs. The entire structure was built trying to reach a good compromise between stiffness, strength and lightness in order to ensure that affect as little as possible the imposed motion from the shaker.

Figure 4.9 shows the IPMC strip mounted on the prototype fabricated.

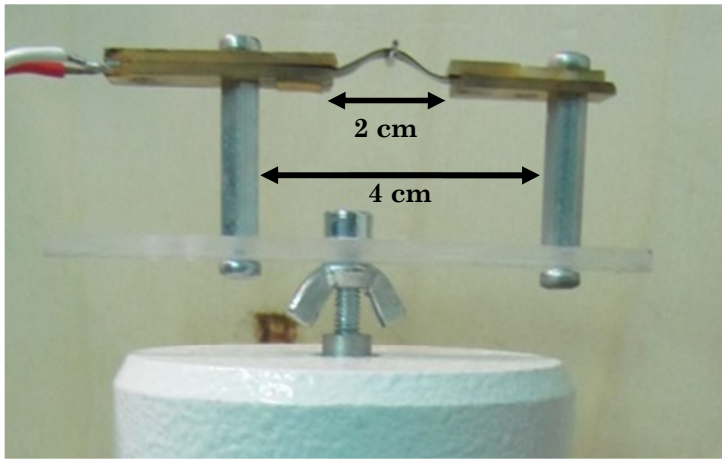

Figure 4.9: Prototype fabricated

The entire test prototype is mounted on a shaker system for vibration testing.

The distance between the two clamps in which the membrane is stucked is equal to 2 cm.

The membrane was deliberately bent in order to obtain a maximum excursion, during the passage between a point of stability to another, approximately 1 cm.

For the study conducted in this work has been used a IPMC membrane soaked in ethylene glycol. The IPMC membrane was cutted obtaining a strip with sizes equal to 3.5 cm x 5 mm.

A first measurement campaign was carried out. But in this campaign, due to the lightness of the material and the amplitude of the oscillations imposed, deliberately kept low in order to simulate ambient vibrations of low intensity, did not occurred the transition between the states of stability.

The bistability was observed after the insertion into the system of an inertial mass of 60 mg in the middle point of the membrane, as highlighted in Figure 4.10

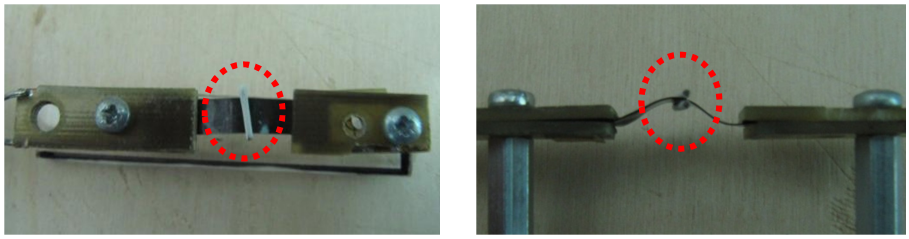

Figure 4.10: Inertial mass added

3.2. Results

Due to the nonlinear nature of the system, in order to analyze his behavior, it was decided to stimulate the device with a series of sinusoidal signals.

The amplitude of the oscillations was kept constant approximately 500 μm and for each acquisition were acquired 10 s.

Each acquisition differed from the others only for the frequency of the applied signal.

In fact, was analyzed the frequency range between 10 Hz and 100 Hz. The frequency of each signal was increased by 10 Hz compared to the previous signal, except in the range between 55 Hz and 85 Hz in which the frequency gaps have been reduced to 2 Hz.

For each stimulating signal, have been acquired both the output short circuit current and the output open circuit voltage, Figure 4.11 shows an example of the signals collected during the measurement campaign. In particular the content of the figure represents an excerpt of the acquired signals obtained by applying a sinusoidal oscillation with frequency equal to 69 Hz.

The curve in blue represents the short-circuit current produced by the IPMC membrane while the green curve represents the real oscillation imprinted by the shaker. The real oscillations were measured by using the laser distance sensor Baumer Electric: OADM 12I6430/S35A.

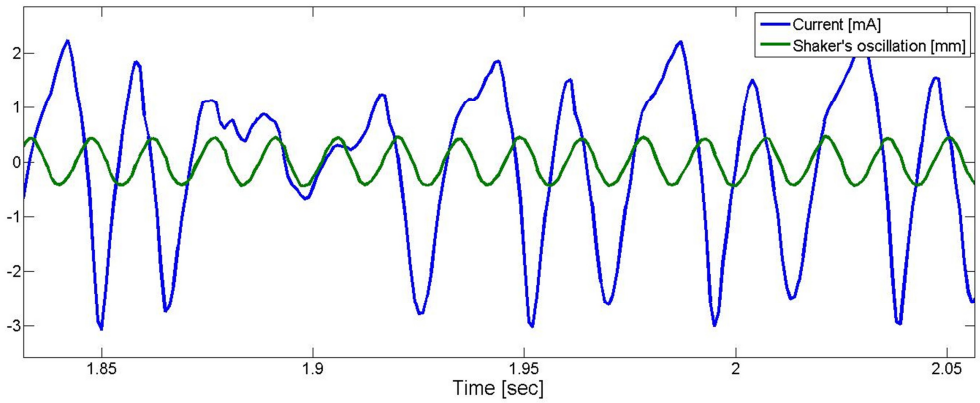

Figure 4.11: Comparison between the shaker's oscillations and the IPMC output current

The system behaviors (frequency response) in different operating conditions are reported in Figure 4.12. In particular in Figure 4.12 a comparison between the power spectral density of the open circuit voltage of the signals obtained by using the same IPMC membrane mounted in the measure system with a linear approach (cantilever beam configuration) and with the non linear approach is showed.

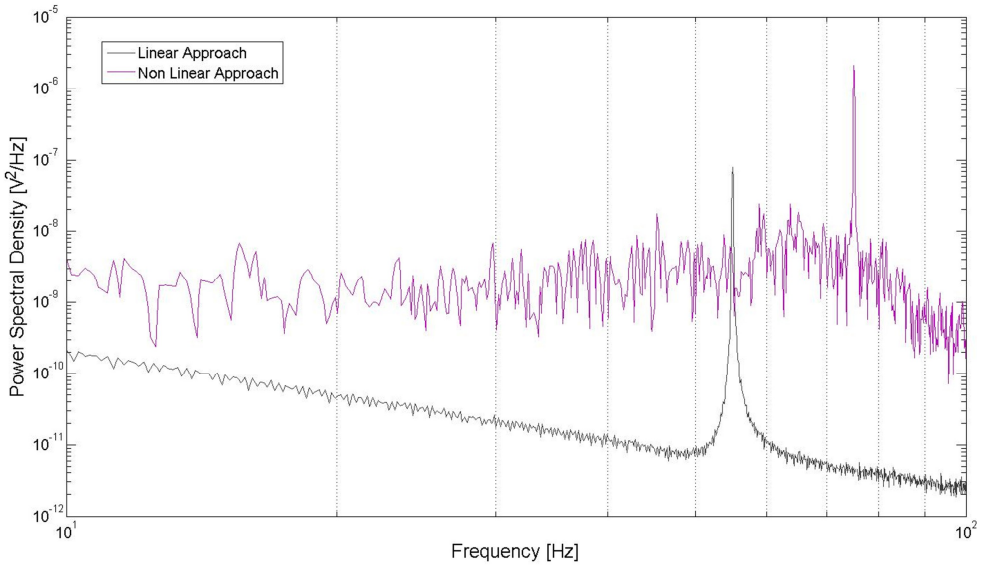

Figure 4.12: Power spectral density associated to the open circuit voltages

From inspection of Figure 4.12 it is possible to note how the response of the membrane placed in bistable configuration (shown in purple) to which has been applied, through a shaker, a solicitation having a frequency equal to 75 Hz, is greater then the response obtained with the same membrane placed in cantilever beam configuration.

In particular, with the bistable configuration we get an harmonic contribution of the output signal in terms of both bandwidth and amplitude.

Similar results are showed on Figure 4.13, where the comparison of the power spectral density associated to the short circuit currents released by the IPMC membrane placed in both configurations same as above is showed

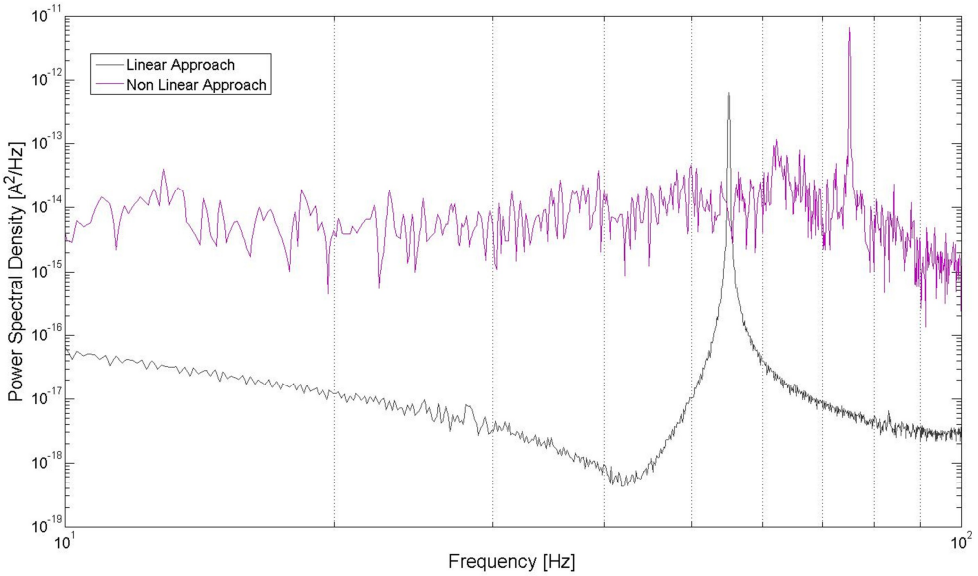

Figure 4.13: Power spectral density associated to the short circuit currents

Also in that case with the bistable configuration it is possible to collect signals greater then the linear configuration.

The spectral response wider than the linear one allows to operate were the frequency response matches more closely what is available in the environment.

although the comparison done previously, shown in the Figure 4.12 and Figure 4.13, has provided interesting results, in order to give an overall view has been necessary to plot in a single graph all the curves obtained.

It was decided to use a "contours map", where the coordinate X represents the "input signal frequencies", the coordinate Y "output signal frequency" and with different colors are shown the intensities of the "resulting signals".

Figure 4.14 and Figure 4.15 show the power spectral densities respectively of the open circuit voltage signals and of the short circuit current signals.

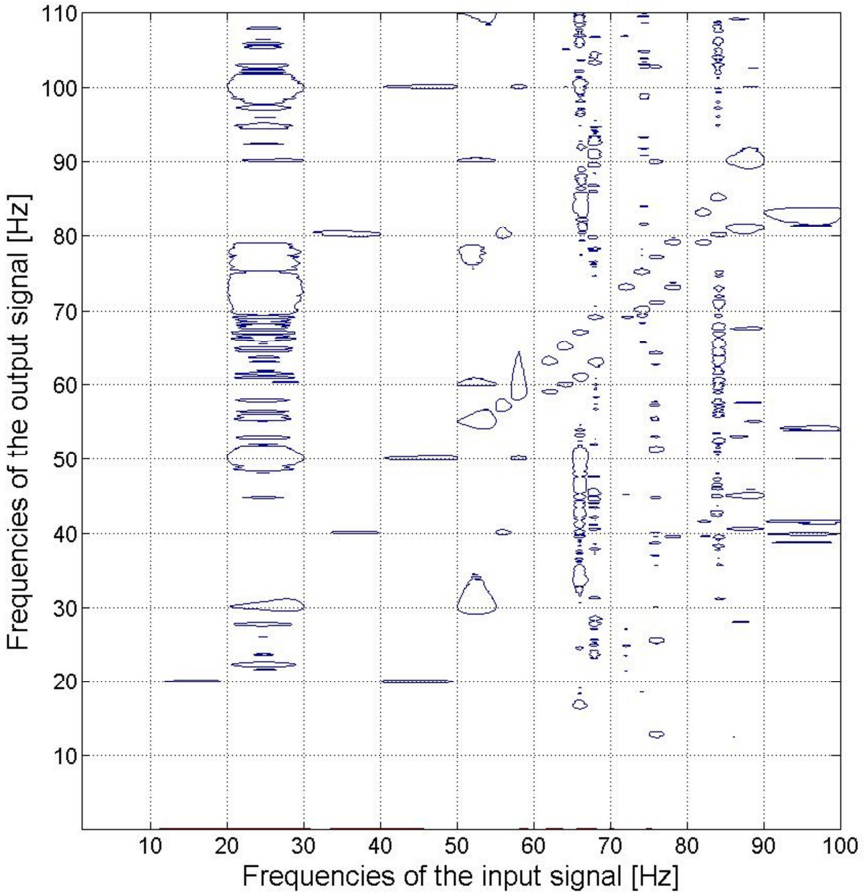

Figure 4.14: Power spectral density of the open circuit voltage signals

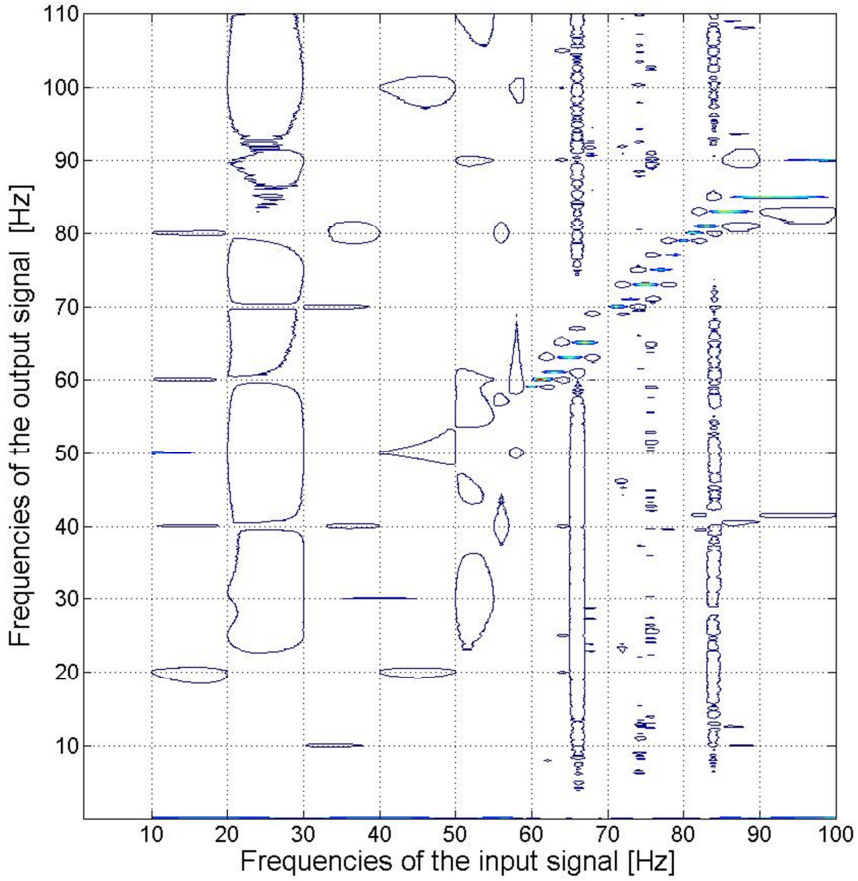

Figure 4.15: Power spectral density of the short circuit current signals

Observing the figures above it is possible to notice that for applied signals having frequencies in the range between 60 Hz and 85 Hz, the device assumes a bistable behavior.

This demonstrates that the bistable configuration improve the harvesting capabilities, because both the amplitude of the generated signals and the sensible bandwidth are increases.

4. Conclusions

The power harvesting properties of a novel class of polymeric transducers, i.e. IP²Cs in air, are investigated and compared to the performances of IPMCs, whose performances have been already investigated in the literature.

Reported results show that the proposed technology compares favorably in the considered frequency range.

Though the developed power is lower than power attainable by using more traditional technologies such as piezoelectric devices, reported results shown interesting enhancements with respect to the performance of IPMCs as power harvesters. Though further improvements are necessary, IP²C could be of interest to realize all polymeric powering devices and even low power wireless sensor networks.

Since IP²Cs are reversible electromechanical devices the possibility to realize all polymeric autonomous smart devices is foreseen.

In addition to the research with new materials, also the comparison of the behavior of the IPMC membranes used as powr harvester and placed in different configurations has been performed.

In particular it has been shown that a bistable configuration improve the harvesting capabilities, because both the amplitude of the generated signals and the sensible bandwidth are increases.

Though the technology used is still room for improvement, the idea to harvest energy from ambient vibrations look feasible.

Research Conclusions

The purpose of this thesis is the development and analysis of smart systems based on electroactive polymers (EAPs). For this dissertation, I successfully implemented a total of three applications based on electroactive materials.

I used both IPMC and IP²C devices, and my focus was on study the feasiblity to realize smart systems with a plastic based electronics able to open new possibilities for a post-silicon era.

I decided to use these materials due to their characteristics such as flexibility, lightness, low voltage activated and low cost. In addition, IP²C are completely made of plastic materials.

I spent my time fabricating and modeling the response of all the systems that I have implemented, using the laboratory equipment that the faculty of engineering of the University of Catania has allowed me to use. Though, for each application investigated, I ended up implementing my own separate experimental set-ups that comprise:

- containment structures, *for simulate the environmental conditions*
- conditioning circuits, *for conditioning the signals collected or derivered to the electroactive devices*
- scheme with my own LabVIEW code, *for data acquisitions*
- own MABLAB code, *for the post processing*

In order to achieve totally polymeric systems, have been designed and studied two sensors (viscometer and seismic sensor) and a power supply system that use renewable sources.

The first device analized was the viscometer. It uses the electromechanical characteristics of a vibrating system at the resonance frequen-

cy, to determine the density and the viscosity of the fluid in which is immersed. It is because the behaviour of a cantilever beam immersed in a fluid strictly depend by the characteristics, like densities and viscosities, of the fluid in wich it is immersed. This device as been proposed in two versions.

The system, in its first version, involves the use of an actuator IPMC set in vibration, by applying an ad hoc voltage signal. To measure the amplitude and frequency of the deflection produced by the actuator it was used a distance laser sensor.

This first version represents a prototype intermediate aimed at demonstrating the possibility to realize a viscometer using IPMC transducers, it was intended as a proof of concept and was of no practical application.

In the second version the IPMC actuator is still used to impose a vibration to the whole system, but the laser distance sensor is replaced by an IPMC sensor attached to the actuator so that it is forced to follow the system deflection, that allow the measurement of the deformation of the vibrating actuator.

With this change now the device consist in a multilayer beam realized superimposing an IPMC actuator and an IPMC sensor. The system is freed by external devices, such as the laser sensor to make the measurements, allowing the realization of a smart system, totally polymeric, able to provide directly an output signal, useful for the estimation of the rheological parameters of the fluid in applications of real interest.

This signals are collected and processed to perform the measurement of the deflection, from this information it is possible to obtain the values of the system's resonant frequency and its quality factor and from these to trace the rheological characteristics of the fluid. The obtained results show the applicability of the proposed systems.

The second device analized was a seismic sensor based on the interaction between a IPMC and a ferrofluid. Main advantage of the proposed sensor is related to the possibility to purposefully tune the sensor behavior (e.g. operating range, frequency bandwidth and responsivity) by control an external magnetic field. Though, applications exist where the seismic sensor is intended as an ad-hoc device required to measure

vibration with established characteristics, working conditions can be envisaged where the required sensor specifications need to be changed according to the mechanical solicitation or the application scenario.

Combining performances of IPMC sensors and magnetic fluid properties it is possible to optimize the sensor performances in terms of its operating range, sensitivity and frequency response, adapting it to the characteristics to the specific application under investigation.

Experimental results demonstrate that the sensor behavior depends on the fluid density and its specifications can be tuned by an external magnetic field.

A model has been presented to predict the system behavior as a function of the effect of the external magnetic field on the ferrofluid density.

The third and last application proposed, important for the purpose of the thesis because it allows to obtain devices electrically independent and then completes the research on the possibility of achieving all smart polymeric systems, is the power harvesting properties of the electroactive deviced used (IPMCs and IP^{2}Cs)

Though the developed power is lower than power attainable by using more traditional technologies such as piezoelectric devices, reported results shown interesting enhancements with respect to the performance of IPMCs as power harvesters. Though further improvements are necessary, IP^{2}C could be of interest to realize all polymeric powering devices and even low power wireless sensor networks.

Since IP^{2}Cs are reversible electromechanical devices the possibility to realize all polymeric autonomous smart devices is foreseen.

In addition to the research with new materials, also the comparison of the behavior of the IPMC membranes used as power harvester and placed in different configurations has been performed.

In particular it has been shown that a bistable configuration improve the harvesting capabilities, it is because both the amplitude of the generated signal and the sensible bandwidth are increases.

Reported results has allowed to assert that, proposed technology compares favorably in the considered frequency range and although the

technology used is still room for improvement, the idea to harvest energy from ambient vibrations is feasible.

All set of experiments shows the applicability of the proposed idea aim of the thesys, which is to develop and analyze smart systems based on electroactive polymers in order to synthesize new all-polymeric systems able to open new possibilities for a post-silicon era.

APPENDIX

1. Viscometer

1.1. Concentrative Properties Of Sucrose Solutions $C_{12}H_{22}O_{11}$

Mass %	*m/mol kg^{-1}*	*c/mol L^{-1}*	*ρ/g cm^{-3}*	*n*	*Δ/°C*	*η/mPa s*
0.5	0.015	0.015	10.002	13.337	0.03	1.015
1.0	0.030	0.029	10.021	13.344	0.06	1.028
2.0	0.060	0.059	10.060	13.359	0.11	1.055
3.0	0.090	0.089	10.099	13.373	0.17	1.084
4.0	0.122	0.118	10.139	13.388	0.23	1.114
5.0	0.154	0.149	10.178	13.403	0.29	1.146
6.0	0.186	0.179	10.218	13.418	0.35	1.179
7.0	0.220	0.210	10.259	13.433	0.42	1.215
8.0	0.254	0.241	10.299	13.448	0.49	1.254
9.0	0.289	0.272	10.340	13.463	0.55	1.294
10.0	0.325	0.303	10.381	13.478	0.63	1.336
12.0	0.398	0.367	10.465	13.509	0.77	1.429
14.0	0.476	0.431	10.549	13.541	0.93	1.534
16.0	0.556	0.497	10.635	13.573	1.10	1.653
18.0	0.641	0.564	10.722	13.606	1.27	1.790
20.0	0.730	0.632	10.810	13.639	1.47	1.945
22.0	0.824	0.700	10.899	13.672	1.67	2.124
24.0	0.923	0.771	10.990	13.706	1.89	2.331

Mass %	m/mol kg^{-1}	c/mol L^{-1}	ρ/g cm^{-3}	n	Δ/°C	η/mPa s
26.0	1.026	0.842	11.082	13.741	2.12	2.573
28.0	1.136	0.914	11.175	13.776	2.37	2.855
30.0	1.252	0.988	11.270	13.812	2.64	3.187
32.0	1.375	1.063	11.366	13.848	2.94	3.762
34.0	1.505	1.139	11.464	13.885	3.27	4.052
36.0	1.643	1.216	11.562	13.922	3.63	4.621
38.0	1.791	1.295	11.663	13.960	4.02	5.315
40.0	1.948	1.375	11.765	13.999	4.45	6.162
42.0	2.116	1.456	11.868	14.038	4.93	7.234
44.0	2.295	1.539	11.972	14.078		8.596
46.0	2.489	1.623	12.079	14.118		10.301
48.0	2.697	1.709	12.186	14.159		12.515
50.0	2.921	1.796	12.295	14.201		15.431
60.0	4.382	2.255	12.864	14.419		58.487
70.0	6.817	2.755	13.472	14.654		481.561
80.0	11.686	3.299	14.117	14.906		

1.2. error minimization algorithm for the search of the parameters of the IPMC sensor

```
close all
clc

AAA=who;

global ti_s b_s Ls_s tresh1 tresh2     f2 fft_def N fft_cor w
Txy F

%------------------------- DICHIARAZIONI --------------------
-------------

ti_s=0.0002;  %spessore 117Na
b_s=0.0015;    %larghezza
Ls_s=0.022;   %lunghezza applicazione cella di carico
```

```
T=30; %durata dei singoli segnali
Fcamp=1000; %Frequenza di campionamento



%-------Stimo le medie delle fft della deformazione e della
corrente------
S1=length(AAA);
for n=1:S1
    M = cell2mat(AAA(n));
    eval(['B=' M ';'])
    fft_def1(:,n)=fft(B(:,4));
    fft_cor1(:,n)=fft(B(:,3));
    [Txy1(:,n),F] = TFESTIMA-
TE(B(:,4),B(:,3),1024*8,[],[],Fcamp);
end
fft_def=mean(abs(fft_def1),2); %calcola la fft della deforma-
zione media
fft_cor=mean(abs(fft_cor1),2); %calcola la fft della corrente
media
Txy=mean(abs(Txy1),2);

clear AAA S1 n M B Txy F fas Sfasamento mod fase fase1 mod1;
%-----------------------------------------------------------
-------------

N = T*Fcamp;
df = 1/(N/Fcamp);
f2 = (1:N/2-1)*df;

tresh1=find(f2>10); %limite inferiore in frequenza per l'ela-
borazione
tresh2=find(f2>25); %limite superiore in frequenza per l'ela-
borazione

w=2*pi*f2;

init=[-2.2232735e+004  3.0748994e+009  4.5393244e+006];
options = optimset('TolX',1e-
12,'MaxIter',Inf,'MaxFunEvals',Inf);
valore=fminsearch('errore_modello_sensore',init,options);

save valore_sens.txt valore -ascii
```

```
clear Fcamp Ls_s N T Txy1 b_s df f2 fft_cor fft_cor1 fft_def
fft_def1 init options ti_s tresh1 tresh2 valore w



function err = errore_modello_sensore(valore)

global ti_s b_s Ls_s tresh1 tresh2 f2 fft_def N fft_cor w Txy
F

Y_s=1e9;

k_s=abs(valore(1));
p1_s=abs(valore(2));
p2_s=abs(valore(3));

d=k_s./((1i*w+p1_s).*(1i*w+p2_s));
sensore=(1i*w).*(3*d.*ti_s*b_s*Y_s)./(4*Ls_s);

def_f_sens=sensore.*fft_def(1:N/2-1)';


err=sqrt(sum(abs(abs(def_f_sens(tresh1(1):tresh2(1)))-
abs(fft_cor(tresh1(1):tresh2(1))' )).^2))
%err=sqrt(sum((abs(sensore(tresh1(1):tresh2(1)))-
abs(Txy(tresh1(1):tresh2(1))' )).^2))


subplot(2,1,1)
plot(f2(tresh1(1):tresh2(1)),abs(def_f_sens(tresh1(1):tresh2(
1))),f2(tresh1(1):tresh2(1)),abs(fft_cor(tresh1(1):tresh2(1))
));
    ylabel('Sensing Current')
subplot(2,1,2)
plot(f2(tresh1(1):tresh2(1)),sensore(tresh1(1):tresh2(1)),F,T
xy)
    ylabel('i/delta')
    axis([f2(tresh1(1)) f2(tresh2(1))
0.7*min(sensore(tresh1(1):tresh2(1)))
1.3*max(sensore(tresh1(1):tresh2(1)))]);

pause(0.1)
end
```

1.3. search algorithm of the rheological parameters of the fluid

```
%Fa il grafico della curva media di modulo e fase di tutto
ciò che è contenuto nel workspace

AAA=who;

global w s h b L fxp xpdef tresh1 tresh2 tresh3 tresh4 rhoe-
ta_interpolata

load rhoeta_interpolata.txt

S1=length(AAA);
Sfasamento = zeros(S1,1);


ti_s=200e-6;  %spessore 117Na
b_s=1.5e-3;    %larghezza
Ls_s=20e-3;   %lunghezza applicazione cella di carico
Y_s=1e9;

par=load('valore_sens.txt');
k_s=abs(par(1));
p1_s=abs(par(2));
p2_s=abs(par(3));



for n=1:S1
    M = cell2mat(AAA(n));
    eval(['B=' M ';'])
    [TxyAA(:,n),fxp] = TFESTIMA-
TE(B(:,2),B(:,3),1024*8,[],[],1000);

    w=2*pi*fxp;
    d=k_s./((1i*w+p1_s).*(1i*w+p2_s));
    sensore=(1i*w).*(3*d.*ti_s*b_s*Y_s)./(4*Ls_s);

    Txy(:,n)=(1./sensore).*TxyAA(:,n);

    fas=((phase(Txy(:,n))))*(180/pi);
    Sfasamento(n)=floor(fas(165)/360);
    mod(:,n)=(abs(Txy(:,n)));
    fase(:,n)=((phase(Txy(:,n))))*(180/pi)-
(Sfasamento(n))*360;
```

```
end

fase1=mean(fase,2);
xpdef=mean(mod,2);

% clear AAA S1 n M B Txy fas Sfasamento mod fase fase1;

% con UNA BUSTINA DI ZUCCHERO CORRISPONDE AD UNA CONCENTRA-
ZIONE DI ZUCCHERO PARI A 0.03

%
% load sw10mHz50Hz50s1050sr.txt;
% def_1b=sw10mHz50Hz50s1050sr(:,3)-
mean(sw10mHz50Hz50s1050sr(:,3));
% tens_1b=sw10mHz50Hz50s1050sr(:,1)-
mean(sw10mHz50Hz50s1050sr(:,1));
% [xpdef,fxp]=tfestimate(tens_1b,-
0.0016*def_1b,[],[],[],1050);

w=2*pi*fxp;
s=1i*w;


h=3.0289771e-004%333e-6;
b=4e-3;
L=26e-3;

% h=333e-6;
% b=4e-3;
% L=30e-3;

tresh_1=find(fxp>10);%4 sugar30
tresh_2=find(fxp>20);%7 sugar30
tresh1=tresh_1(1);
tresh2=tresh_2(1);

% tresh_3=find(fxp>20);%4 sugar30
% tresh_4=find(fxp>25);%7 sugar30
% tresh3=tresh_3(1);
% tresh4=tresh_4(1);



init=[1111 3e-3]; %rho_f eta_f
```

```
options = optimset('TolX',1e-
12,'MaxIter',2000,'MaxFunEvals',2000);
valore=fminsearch(@errore,init,options);
save aaaa.txt valore -ascii



% clear w s h b L fxp xpdef tresh1 tresh2 init tresh_1
tresh_2 valore options rhoeta_interpolata tresh3 tresh4 init
tresh_3 tresh_4 ;


function err = errore(par)

global w s h b L fxp xpdef tresh1 tresh2 tresh3 tresh4 rhoe-
ta_interpolata


 rhof=abs(par(1));
 eta=abs(par(2));
%kk=abs(par(1));

% index=find(rhoeta_interpolata(:,1)>abs(par(1)));
% rhof=rhoeta_interpolata(index(1),2);
% eta=rhoeta_interpolata(index(1),3);




% rhof=998.29;           %densità acqua a 25 gradi [kg/mc]
% eta=1.003e-3; %viscosità acqua a 25 gradi [Pa s ]

Ke=3.74e-7; %F/m
F=96487; %C/mol
R=8.3143; %J/(mol*K)
T=300; %K
Cm=1200; %mol/m3

% d=abs(par(1));
% h=abs(par(2));

d=1.0283034e-003;
% d=4.6994e-011;
%d=8.1652e-011;
```

```
%d=1.030*10^(-10);

K=(F^2*d*Cm)./(Ke*R*T);
Beta2=(1/d).*(s+K);
Beta=sqrt(abs(Beta2));
Gamma=0.5*h*Beta;
C=((b*L)/(h)).*Ke;
Z=(s+(K.*(tanh(Gamma)./Gamma))).(C.*s.*(s+K));

Rdc=330*((2*h)/(L*b));
Z1=(Rdc*Z)./(Rdc+Z);
alfa0=2.9102223e-001*(1./((1+(2.5466484e-
010*s)).*(1+(3.1599113e-
010*s))));%??????????????????????????%alfa0=0.6029*(1./((1+(
0.0031*s)).*(1+(0.0000084*s))));%??????????????????????????
M=-4.2*b*alfa0.*Ke.*K.*((Gamma-tanh(Gamma))./(s.*Gamma-
K.*tanh(Gamma)));  %% Paola,queste prime righe andrebbero su-
stituite con la fdt dell'attuatore che
%%usi tu
%


J=(b*h^3)/12;
E=0.24*10^9;
rho=2300;      %Densità del Nafion [kg/m^3]
S=b*h;         %Sezione della trave
a=(E*J)/(rho*S);
%
Cs=0.003;




load c_real.mat
load c_imag.mat
a1=c_real(1);
a2=c_real(2);
b1=c_imag(1);
b2=c_imag(2);


% a1= 1.053;
% a2= 3.7997;
% b1= 3.8018;
% b2= 2.7364;
```

```
%
lambda = (1/L)*[1.8751 4.6941   7.854];
%
md=0.25*pi*rhof*b^2; %massa x unità di lungheza fluido
m=rho*S; %massa x unità di lunghezza IPMC
%

k1=(4/(m+md));

for j=1:3
    beta(j)=(sinh(lambda(j)*L)-
sin(lambda(j)*L))/(cosh(lambda(j)*L)+cos(lambda(j)*L));
    w_ris(j)=sqrt(a)*(lambda(j))^2;
    fris=w_ris/(2*pi);
    w_ris_f(j)=w_ris(j)*(1+(pi*rhof*b)/(4*rho*h))^(-0.5);
    fris_f=w_ris_f/(2*pi);
    deltan(j)=sqrt((2*eta)/(rhof*w_ris_f(j)));
    gammare(j)=(a1+a2*(deltan(j)/b));
    gammaim(j)=b1*(deltan(j)/b)+b2*(deltan(j)/b)^2;

dmp_f(j)=(Cs+md*w_ris_f(j)*gammaim(j))/((m+gammare(j)*md)*w_r
is_f(j));
    Hf(j,:)=1./(1-
(w/w_ris_f(j)).^2+(i*2*dmp_f(j)*(w/w_ris_f(j))));

defl_f(j,:)=k1*((lambda(j)*beta(j))/(w_ris_f(j))^2).*Hf(j,:).
*M';
    q1=(4*eta)/(pi*rhof*b^2);
    Q(j,:)=(q1+gammare(j))./(gammaim(j));
  end
def_f=sum(defl_f)';
%def_f=sum((defl_f)/kk)';

err1=sqrt(sum(abs(abs(def_f(tresh1(1):tresh2(1)))-
abs(xpdef(tresh1(1):tresh2(1)))).^2));
%err2=sqrt(sum(abs(abs(def_f(tresh3(1):tresh4(1)))-
abs(xpdef(tresh3(1):tresh4(1)))).^2))*2;
err=err1

rhof
eta
%rhoeta_interpolata(index(1),1)
d
```

```
figure(10) %%%
% subplot(2,1,1);
plot(fxp,abs(def_f),fxp,abs(xpdef))%,fxp,abs(xpdef_1b),fxp,ab
s(xpdef_2b),fxp,abs(xpdef_sat))
    axis([1 30 0 0.001])
    grid on
% subplot(2,1,2)
%
plot(fxp,(180/pi)*((unwrap(angle(defl_f(1,:)))+unwrap((angle(
defl_f(2,:)))))),fxp,(180/pi)*unwrap(angle(xpdef)))
```

2. Power Harvesting

2.1. Trova FDT Sub

%load S1.txt; % Il file S1.txt contiene la misura della deformazione meccanica del
% subwoofer a seguito dell'applicazione di un treno di sweep sinusoidali lineari
% frequenza iniziale 1 Hz e finale 100 Hz, durata di 120 s, frequenza
% di campionamento 10 kHz. Mediante tale misura si ricava la f.d.t del
% sistema subwoofer (deformazione meccanica-tensione di ingresso[mm/V]) per
% f che va da 1 a 100 Hz

Fs = 5000; % Frequenza di campionamento
Tsweep = 30; % Periodo dello sweep utilizzato per valutare la f.d.t.
laser = 1; % Fattore di conversione laser
Sv = zeros (5, Fs*Tsweep); % Preallocazione di memoria
Sd = zeros (5, Fs*Tsweep); % " "
TdV = zeros(5, 4097); % " "

% Sezionamento delle misure
 for k=1:3
Sv(k, :) = detrend(S2((Fs*Tsweep*(k-1)+1):(Fs*Tsweep*k), 1));
Sd(k, :) = detrend(S2((Fs*Tsweep*(k-1)+1):(Fs*Tsweep*k), 4))*laser;

```
[TdV(k, :), F] = tfestimate(Sv(k, :), Sd(k, :), 8192, [], [], Fs);
end

TS = mean(TdV, 1); % TS è valutata come f.d.t media tra quelle dei 5 periodi di misura analizzati

TSabs = abs(TS);

indexF = find(F>100);

semilogx(F, TSabs)
title ('Funzione di trasferimento Subwoofer')
xlabel('Frequenza[Hz]')
ylabel('Gain Magnitude(abs)')
axis([min(F) 100 0 1.1*max(TSabs(1:indexF(1)))]); % Settaggio degli assi
grid on

save ('TF.mat', 'TS', 'TSabs', 'F');
```

2.2. Genera segnale Sub

```
% Con questo script si costruisce un segnale costituito da un treno di
% sinusoidi, ciascuna di durata pari a un periodo, a frequenza crescente
% con step impostato dall'utente (non inferiore ad 1 Hz). La frequenza
% finale è fissata a 100Hz. L'ampiezza delle sinuosidi varia con la
% frequenza in modo da compensare il guadagno del sub-woofer. Il segnale
% generato, infine, è un segnale normalizzato rispetto all'ampiezza
% massima, tale che, passando attraverso il sub-woofer,
% in'uscita si abbia una deformazione meccanica costituiuta da un treno di
% sinusoidi ad ampiezza costante.

load Tf.mat % Viene caricato il workspace con i dati necessari allo script.
```

```
% Ts è la f.d.t del subwoofer valutata per frequenze da 1.221 a 100Hz, con
% step pari a circa 1.22Hz, che può essere un valore troppo grande. La TS è
% nota per tali valori di e non altrove!
%
% Tabs è il modulo di TS (non in dB).

step = inputdlg('Step[Hz]'); % Step impostato dall'utente
fs = inputdlg('Pseudo-Sampling Frequency[Hz]'); % Frequenza di campionamento impostata dall'utente
step = str2double(step{1}); % Conversione da stringa a numero
fs = str2double(fs{1}); % Conversione da stringa a numero

Fi = 1:step:5000; % Questo valore non va modificato
Fstart=5; %deve essere un numero intero
Fmax = 100; % questo valore non va modificato

[A, B]=cheby1(10, 0.1, 0.2);
TTf = filtfilt(A, B, TSabs(1, :)); % La TSabs viene filtrata attraverso un filtro di Chebychev passa-basso del decimo ordine e con 0.1db di ripple
% banda passante, per ottenere un effetto di smooth.
TSi = interp1(F, TTf, Fi, 'linear'); % Tsi è l'interpolazione lineare della TTf con step inserito dall'utente.
% Con tale step verrà costruito il segnale da inviare al generatore di
% funzioni e dato a sua volta allo shaker.
ITSi = 1./TSi; % ITSi è l'inversa di TSi.

VinGen = 0; % Memory preallocation

% Costruzione del segnale
for i = Fstart:(Fmax-1)/step+1
t = 0:1/fs:(1/(1+step*(i-1)))-1/fs;
eval(['A', num2str(i), '=ITSi(i)*sin(2*pi*Fi(i)*t);']);
eval(['VinGen = [VinGen, A', num2str(i), '];']);
```

```
eval(['clear A', num2str(i), ';']);
end

frequenza_segnale_in_mHz = fs/length(VinGen)*1000 % Questo valore va impostato nel generatore di funzioni

tempoVinGen = 0:1/fs:length(VinGen)/fs-1/fs; % Durata temporale dell'intero segnale

VinGen = VinGen/max(VinGen); % A noi interessa il segnale normalizzato, e comunque questa operazione la compirebbe il generatore di funzioni stesso

% Andamento temporale del segnale generato
plot(tempoVinGen, VinGen)
title ('Vin Generatore')
xlabel('Tempo[s]')
ylabel('Tensione di ingresso normalizzata[V]')
axis([0 length(VinGen)/fs -1 1])
grid on

VinGen = (VinGen)'; % LabView vuole un vettore colonna, non un vettore riga
save VinGen.txt VinGen -ascii; % Salvataggio del segnale generato
```

2.3. script used for processing the non-linear system data obtained from acquisitions

```
AAA=who;
S1=length(AAA);

g=501;
Fs = 1000;

for n=1:S1
 M = cell2mat(AAA(n));
```

```
 eval(['nfft = 2^nextpow2(length(' M '(:, 1)/g));'])
 eval(['Pxx(:, n) = abs(fft(' M '(:, 1)/g, nfft)).^2/length('
M '(:, 1))/Fs;'])
 upperind = find(diff(sign(diff(Pxx(:, n)))) < 0) + 1;
f = 1;
l = length(Pxx(:, n));
try
 upperind = [f upperind l];
catch
 upperind = [f; upperind; l];
end
xi = f : l;
upperenv(:, n) = interp1(upperind, Pxx(upperind, n), xi,
'linear', 'extrap');
clear upperind
end

ii=0:1/nfft*1000:1000;
i=ii(1:end-1)
[X, Y] = meshgrid(i, frequenze);
%surf(Y', X', Pxx(1:16384, :))
[xi, yi] = meshgrid(i, 1:1:100);
contour(xi', yi', upperenv)
```

BIBLIOGRAPHY

[1] M. Shahinpoor and K. J. Kim, "Ionic polymer-metal composites: I. Fundamentals," *Smart Materials and Structures,* vol. 10, pp. 819-833, 2001.

[2] P. Millet, R. Durand, E. Dartyge, G. Tourillon and A. Fontaine, "Precipitation of metallic platinum into Nafion ionomer membranes. I. Experimental results," *J. Electrochem. Soc,* vol. 140, no. 5, pp. 1373-1380, 1993.

[3] . K. M. Newbury, Characterization, Modeling, and Control of Ionic Polymer Transducers, PhD Dissertation, Blacksburg, VA: Virginia Polytechnic Institute, 2002.

[4] K. Sadeghipour, R. Salomon and S. Neogi, "Development of a novel electrochemically active membrane and 'smart' material based vibration sensor/damper," *International Journal of Smart Materials and Structures,* vol. 1, no. 2, pp. 172-179, 1992.

[5] K. Oguro, Y. Kawami and H. Takenaka, "An actuator element of polyelectrolyte gel membrane-electrode composite," vol. 43, no. 1, pp. 21-24, 1992.

[6] M. Mojarrad and M. Shahinpoor, "Ion exchange membrane-platinum composites as electrically controllable artificial muscles," *Third International Conference on Intelligent Materials, SPIE Proc.,* vol. 2779, pp. 1012- 1017, 1996.

[7] R. Kanno, A. Kurata, S. Tadokoro, T. Takamori and K. Oguro, "Characteristics and modeling of ICPF actuator," *Proceedings of the Japan-USA Symposium on Flexible Automation,* p. 219–225, 1994.

[8] S. Nemat-Nasser and S. Zamani, "Experimental Study of Nafion- and Flemion- Based Ionic Polymer-Metal Composites (IPMC's) with Ethylene Glycol as Solvent," *Proceedings of SPIE,* vol. 5051, pp. 233-244, 2003.

[9] S. Nemat-Nasser and J. Y. Li, "Electromechanical response of ionic polymer-metal composites," *Journal of Applied Physics,* vol. 87, no. 1, pp. 3321-3331, 2000.

[10] S. Nemat-Nasser, "Micromechanics of Actuation of Ionic Polymer-metal Composites," *Journal of Applied Physics,* vol. 92, no. 5, pp. 2899-2915, 2002.

[11] S. Nemat-Nasser and Y. Wu, "Comparative Experimental Study of Nafion-and-Flemion-Based Ionic Polymer-metal Composites (IPMC)," *Journal of Applied Physics,* vol. 93, no. 9, pp. 5255-5267, 2003.

[12] P. Millet, M. Pineri and R. Durand, "New solid polymer electrolyte composites for water electrolysis," *Journal of Applied Electrochemistry,* vol. 19, no. 2, pp. 162-166, 1989.

[13] P. Millet, R. Durand and M. Pineri, "Preparation of new solid polymer electrolyte composites for water electrolysis," *International Journal of Hydrogen Energy,* vol. 15, no. 4, pp. 245-253, 1990.

[14] P. Millet, "Noble metal-membrane composites for electrochemical applications," vol. 76, no. 1, pp. 47-49, 1999.

[15] M. Shahinpoor and K. J. Kim, "Ionic polymer–metal composites: IV. Industrial and medical applications," *Smart Materials and Structures,* vol. 14, no. 1, pp. 197-214, 2005.

[16] P. De Gennes, K. Okumura, M. Shahinpoor and K. Kim, "Mechanoelectric effects in ionic gels," *Europhysics Letters,* vol. 50, no. 4, p. 513–518, 2000.

[17] S. Tadokoro, S. Yamagami, T. Takamori and K. Oguro, "Modeling of Nafion-Pt composite actuators (ICPF) by ionic motion," *SPIE Proceedings,* vol. 3987, pp. 92-102, 2000.

[18] B. E. Bartrum and (Dow Chemical Co.), "Process for plating permselective membrane". Patent GB: 1, 143, 883, 1969.

[19] A. Wiechen and (Thiele, Heinrich), "Isopor membranes". Patent DE: 1, 303, 142, 1971.

[20] P. Millet, R. Durand, E. Dartyge, G. Tourillon and A. Fontaine, "Study of the precipitation of metallic platinum into ionomer membranes by time resolved dispersive x-ray spectroscopy," *AIP Conference Proceedings,* vol. 258, pp. 531-538, 1992.

[21] R. K. Jain, U. S. Patkar and S. Majumder, "Micro Gripper for Micro Manipulation Using IPMCs," *Journal of Scientific Industrial Research,* vol. 68, pp. 23-28, Jan 2009.

[22] B.-K. Fang, . M.-S. Ju and C.-C. K. Lin, "A new approach to develop ionic polymer–metal composites (IPMC) actuator: Fabrication and control for active catheter systems," *Sensors and Actuators: A Physical,* vol. 137, no. 2, pp. 321-329, 2007.

[23] S. J. Higgins, K. V. Lovell, R. M. G. Rajapakse and N. M. Walsby, "Grafting and electrochemical characterisation of poly-(3,4-ethylenedioxythiophene) films, on Nafion and on radiation-grafted polystyrenesulfonate–polyvinylidene fluoride composite surfaces," *Journal of Materials Chemistry,* vol. 13, pp. 2485-2489, 2003.

[24] E. Malone and H. Lipson, "Freeform fabrication of ionomeric polymer–metal composite actuators," *Rapid Prototyping Journal,* vol. 12, no. 244–253, 2006.

[25] L. Fortuna, S. Graziani, M. La Rosa, D. Nicolosi, G. Sicurella and E. Umana, "Modelling and design of all-organic electromechanic transducers," *The European Physical Journal Applied Physics,* vol. 46, no. 1, p. 12513 (4 pages), 2009.

[26] G. Di Pasquale, L. Fortuna, S. Graziani, M. La Rosa, D. Nicolosi, G. Sicurella and E. Umana, "All organic actuation and sensing devices," in *IEEE Instrumentation and Measurement Technology Conference - I2MTC*, Victoria, Vancouver Island, 2008.

[27] G. Di Pasquale, L. Fortuna, S. Graziani, M. La Rosa, D. Nicolosi, G. Sicurella and E. Umana, "All-organic motion sensors: electromechanical modeling," *IEEE Transactions Instrumentation and Measurement (I2MTC '08 Special Issue),* vol. 58, p. 3731–3738, 2009.

[28] N. Ahmed, D. F. Nino and V. T. Moy , "Measurement of solution viscosity by atomic force microscopy," *Review of Scientific Instruments,* vol. 72, p. 2731–2734, 2001.

[29] C. Bergaud and L. Nicu, "Viscosity measurements based on experimental investigations of composite cantilever beam eigenfrequencies in viscous media," *Review of Scientific Instruments,* vol. 71, p. 2487–2491, 2000.

[30] P. I. Oden, G. Chen, R. A. Steele, R. J. Warmack and T. Thundat, "Viscous drag measurement utilizing microfabricated cantilevers," *Applied Physics Letters,* vol. 68, pp. 3814-3816, 1996.

[31] S. Boskovic, J. W. M. Chon, P. Mulvaney and J. E. Sader, "Rheological measurements using microcantilever," *Journal of Rheology,* vol. 46, pp. 891-899, 2002.

[32] J. E. Sader, "Frequency response of cantilever beams immersed in viscous fluids with applications to the atomic force microscope," *Journal of Applied Physics,* vol. 84, pp. 64-76, 1998.

[33] J. E. Sader, J. W. M. Chon and P. Mulvaney, "Calibration of

rectangular atomic force microscope Cantilevers," *Review of Scientific Instruments,* vol. 70, pp. 3967-3969, 1999.

[34] M. Hennemeyer, S. Burghardt and R. W. Stark, ""Cantilever micro-rheometer for the characterization of sugar solutions," *Sensors,* vol. 8, pp. 10-22, 2008.

[35] P. Brunetto, S. Graziani, S. Strazzeri and M. G. Xibilia, "A small scale viscometer based on IPMCs," in *ICONS 2009*, Istanbul, Turchia, September 2009.

[36] P. Brunetto, L. Fortuna, P. Giannone, S. Graziani and F. Pagano, "A small scale viscometer based on an IPMC actuator and an IPMC sensor," in *IEEE I2MTC*, Austin, Texas, Maggio 2010.

[37] P. Brunetto, L. Fortuna, S. Graziani and S. Strazzeri, "A model of ionic polymer-metal composite actuators in underwater operations," *Smart Materials and Structures,* vol. 17, pp. 1-12, 2008.

[38] C. Bonomo, L. Fortuna, P. Giannone, S. Graziani and S. Strazzeri, "A nonlinear model for ionic polymer metal composites as actuators," *Smart Materials and Structures,* vol. 16, pp. 1-12, 2007.

[39] M. Shahinpoor and K. J. Kim, "Ionic polymer–metal composites: III. Modeling and simulation as biomimetic sensors, actuators, transducers, and artificial muscles," *Smart Materials and Structures,* vol. 13, p. 1362–1388, 2004.

[40] S. Kirstein, M. Mertesdorf and M. Schönhoff, "The influence of a viscous fluid on the vibration dynamics of scanning near-field optical microscopy fiber probes and atomic force microscopy cantilevers," *Journal of Applied Physics,* vol. 84, pp. 1782-1790, 1998.

[41] K. M. Farinholt, Modeling and Characterization of Ionic Polymer Transducers for Sensing and Actuation, Dissertation, Virginia

Polytechnic Institute and State University, 2005.

[42] S. S. Chen, Flow-Induced Vibration of Circular Cylindrical Structures, (Hemisphere, Washington, New York, London, 1987)., 1987.

[43] A. Maali, C. Hurth, R. Boisgard, C. Jai, T. Cohen-Bouhacina and J. Aimè, "Hydrodynamics of oscillating atomic force microscopy cantilevers in viscous fluids," *Journal of Applied Physics,* vol. 97, pp. 074907-1-074907-5, 2005.

[44] G. K. Batchelor, Fluid Dynamics, Cambridge: Cambridge University Press, 1974.

[45] S. S. Rao, Mechanical Vibrations - 4th edition, Prentice Hall, 2003.

[46] C. Bonomo, L. Fortuna, P. Giannone, S. Graziani and S. Strazzeri, "A model for ionic polymer metal composites as sensors," *Smart Materials and Structures,* vol. 15, p. 749–758, 2006.

[47] B. Andò, A. Ascia, S. Baglio and N. Pitrone, "Magnetic fluids and their use in transducers," *IEEE Magazine on Instrumentation and Measurements,* vol. 9, no. 6, pp. 44-47, 2006.

[48] J. Popplewell and R. E. Rosensweig, "Magnetorheological fluid composites," *Journal of Physics D: Applied Physics,* vol. 29, pp. 2297-2303, 1996.

[49] Q. A. Pankhurst, J. Connolly, S. K. Jones and J. Dobson, "Applications of magnetic nanoparticles in biomedicine," *Journal of Physics D: Applied Physics,* vol. 36, p. 167–181, 2003.

[50] B. Andò, S. Baglio, A. Beninato, S. Graziani, F. Pagano and E. Umana, "A seismic sensor based on IPMC combined with ferrofluids," in *IEEE I2MTC Proceedings*, Graz, Austria, 2012.

[51] Corporation, Ferrotec (USA), "http://ferrofluid.ferrotec.com," 2001–2012. [Online]. Available: http://ferrofluid.ferrotec.com.

[52] J. Brufau Penella, M. Puig-Vidal, P. Giannone, S. Graziani and S. Strazzeri, "Characterization of the harvesting capabilities of an ionic polymer metal composite device," *Smart Materials and Structures,* vol. 17, no. 1, 2008.

[53] J. C. Lagarias, J. A. Reeds, M. H. Wright and P. E. Wright, "Convergence Properties of the Nelder-Mead Simplex Method in Low Dimensions," *SIAM Journal of Optimization,* vol. 9, no. 1, pp. 112-147, 1998.

[54] J. A. Paradiso and T. Starner, "Energy Scavenging for Mobile and Wireless Electronics," *IEEE Pervasive Computing,* vol. 4, no. 1, pp. 18-27, 2005.

[55] J. Brufau Penella, Smart materials for micro robotics – Motion control and power harvesting PhD thesis, Universidat de Barcellona, Departament d'electrònica, Facultat de fisica, 2005.

[56] M. Aureli, C. Prince, M. Porfiri and S. D. Peterson, "Energy harvesting from base excitation of ionic polymer metal composites in fluid environments," *IOP Smart Materials and Structures,* vol. 19, no. 15, 2010.

[57] B. J. Akle, M. D. Bennett and D. J. Leo, "High-strain ionomeric–ionic liquid electroactive actuators," *Sensors and Actuators A: Physical,* vol. 126, p. 173–181, 2006.

[58] W. M. Haynes, CRC Handbook of Chemistry and Physics, Boca Raton, FL: CRC Press, 2001.

[59] A. B. Mc Ewen, H. N. Ngo, K. Le Compte and J. L. Goldman, "Electrochemical properties of imidazolium salt electrolytes for electrochemical capacitor applications," *Journal of The Electrochemical Society,* vol. 146, no. 5, p. 1687–1695, 1999.

[60] W. Lu and et al, "Use of ionic liquids for conjugated polymer electrochemical devices," *Science,* vol. 297, p. 983–987, 2002.

[61] Sigma Aldrich, "04367 - EmI-Tf," [Online]. Available: http://www.sigmaaldrich.com/catalog/product/fluka/04367?lang=it&region=IT.

[62] Clevios, "Clevios™ P HC V4," [Online]. Available: http://clevios.com/en/_technik/productdetail_1034008.aspx?psMarketId=1056768&psApplicationId=.

[63] B. Andò, S. Baglio, G. L'Episcopo and C. Trigona, "Investigation on Mechanically Bistable MEMS Devices for Energy Harvesting From Vibrations," *IEEE Journal of Microelectromechanical Systems,* vol. 21, no. 4, pp. 779-790, 2012..

[64] M. Ferrari, V. Ferrari, M. Guizzetti, B. Andò, S. Baglio and C. Trigona, "Improved Energy Harvesting from Wideband Vibrations by Nonlinear Piezoelectric Converters," *Procedia Chemistry,* vol. 1, no. 1, p. 1203–1206, 2009.